Design and Construction of a Propeller Open Water Testing Apparatus and Testing of a Stereolithography 3D Printed Model Propeller.

by

William R. Hentschel

B.S. Marine Engineering Technology, Texas A&M University at Galveston (2012)

Submitted to the Department of Mechanical Engineering
in partial fulfillment of the requirements for the degrees of

Naval Engineer

and

Masters of Science in Mechanical Engineering

at the

MASSACHUSETTS INSTITUTE OF TECHNOLOGY

June 2019

Signature redacted

Author . . . .
Department of Mechanical Engineering
May 6, 2019

Signature redacted

Certified by . . . .
Alexandra Techet
Professor of Ocean and Mechanical Engineering

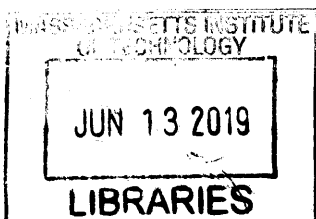Signature redacted Thesis Supervisor

Accepted by . . . .
Nicolas Hadjiconstantinou
Chairman Committee on Graduate Students

Design and Construction of a Propeller Open Water Testing Apparatus and Testing of a Stereolithography 3D Printed Model Propeller.

by

William R. Hentschel

Abstract

This thesis describes the design and construction of a propeller open water testing apparatus for educational and experimental use at MIT. This test apparatus was built as an inexpensive alternative to conducted in-house model scale marine propeller testing. A complimentary study was conducted to explore the process of manufacturing a model propeller using additive manufacturing. A propeller open water test apparatus, commonly referred to as a test boat, is used to measure the performance of marine propellers in uniform flow. The test boats performance was validated using a Wageningen B-series aluminum propeller as a benchmark. The test boat measured the open water performance of this benchmark within a small percentage of error. The practicality of using additive manufacturing to produce a model propeller was explored by manufacturing and testing a 3D printed replica of the benchmark propeller. The replica propeller was manufactured using a benchtop stereolithography 3D printer. The open water characteristics of the replica were measured and compared to the benchmark propeller. Results of this testing revealed some limitations of 3D printed model propellers, such as size constraints and imprecision of propeller blade geometry. This research has provided MIT students with an inexpensive method to conduct preliminary marine propeller testing and offers in-sight into the use of additively manufactured model propellers.

Thesis Supervisor: Alexandra Techet
Title: Professor of Ocean and Mechanical Engineering

Acknowledgments

THIS PAGE INTENTIONALLY LEFT BLANK

Contents

THIS PAGE INTENTIONALLY LEFT BLANK

List of Figures

11

List of Tables

13

THIS PAGE INTENTIONALLY LEFT BLANK

Chapter 1

Introduction

Propeller open water testing is used to characterize the performance of a marine propeller in a uniform flow. The results of these tests are used for full-scale propeller selection or as a foundation for a preliminary propeller design. The open water performance of a propeller can be measured with an apparatus called an open water propeller test boat or in a recirculating water tunnel. The later of which can also be used to test the effects of cavitation by adjusting the absolute pressure in the tunnel. An open water propeller test boat is, in general, a less expensive approach to measuring propeller open water performance. This method also provides the opportunity to test other devices such as tidal turbines and podded propulsors. An open water propeller test boat is a valuable tool for education and research. The purpose of this project is to build an open water propeller test boat to be used in MIT's towing tank. A complimentary study was also conducted to explore the use of additive manufacturing to produce an in-house model-scale propeller.

The project began by designing and building an open water test boat. The test boat was designed with careful consideration of the guidelines and recommendations provided by the International Towing Tank Conference (ITTC). The test boats performance was then validated by measuring the open water performance of a benchmark propeller. The benchmark propeller is a Wageningen B3-70 that was manufactured and tested by Naval Surface Warfare Center Carderock (NSWCC). A 3D printed replica of the benchmark propeller was then manufactured and tested. The replica

propellers geometrical accuracy and open water performance was measured and the result compared to the benchmark. This analysis was used to evaluate the feasibility of producing a model propeller using bench top 3D printing technology.

The goal of this thesis is to build a low-cost open water propeller test boat. This test boat is to be capable of testing model-scale propellers to the requirements set by the ITTC. A subsequent goal is to develop a process to manufacture model propellers in-house using the resources available to MIT students.

MIT's Experimental Hydrodynamics Laboratory has a long history of propeller testing. The facilities main test apparatus is a variable pressure recirculating water tunnel that is capable of speeds up to 10 m/s. In recent years funding for research that utilizes the water tunnel has become scarce and as a result the material condition of the tunnel has degraded. The propeller drive shaft, once used to conducted propeller open water and cavitation testing, is no longer in operations. For these reasons the author was motivated to develop an inexpensive and reliable process to test marine propellers.

1.1   Propeller Theory

The thrust T and torque Q of a propeller can be nondimensionalized either on the bases of ship speed V_S or volumetric mean inflow speed V_A. The preferred method to nondimensionalize thrust and torque results of an open water propeller test is with respect to a nominal rotational velocity, nD, as defined by equations 1.1 and 1.2. This method is preferred because these coefficient remain finite in the case of a static thrust, $V_A = 0$. The ratio of the inflow and rotational velocities, defined by equation 1.3, is called the advance coefficient, or ratio. The following equations are the five primary equations used to express the results of an open water propeller test.

Thrust coefficient:

$$K_T = \frac{T}{\rho n^2 D^4} \tag{1.1}$$

Torque coefficient:

$$K_Q = \frac{Q}{\rho n^2 D^5} \tag{1.2}$$

Advance Ratio:

$$J = \frac{V_A}{nD} \tag{1.3}$$

Propeller efficiency in open water:

$$\eta_o = \frac{J}{2\pi} \cdot \frac{K_T}{K_Q} \tag{1.4}$$

Reynolds number based on chord length at 0.7 radius:

$$Re = \frac{C_{0.7R}(V_A^2 + (0.7\pi nD^2))^{1/2}}{\nu} \tag{1.5}$$

Where

V_A is inflow speed or speed of advance (carriage speed)

T is thrust

n is revolutions per second

Q is torque

D is propeller diameter

ρ is fluid density

R is propeller radius

ν is kinematic viscosity

Values of K_T, K_Q, and η_o with respect to J are plotted on one graph and are known at open water propeller performance curves.

1.1.1   Similitude

Geometric Similarity: The model propeller shape must be the same as the full-scale propeller. Depending on the model size, issues with model blade thickness and leading and trailing edge geometry may arise. Further discussion of these issues will

17

be discussed in a subsequent section. The model to full-scale ratio is defined as.

$$\lambda = \frac{D_S}{D_M}$$

Where D_S is the diameter of the full-scale propeller and D_M is the diameter of the model propeller. Kinematic Similarity: To achieve kinematic similarity the advance ratio J of the model must equal that of the full-scale. This is to insure the direction of the inflow is consistent between the model and full-scale propellers.

Dynamic Similarity: To achieve dynamic similarity Froude and Reynold's laws must by satisfied. The Reynolds number of a propeller is defined by 1.5. The Froude number of a propeller is defined as:

$$F_n = \frac{\pi n D}{\sqrt{gD}}$$

To satisfy both laws would require $n_M = n_S\sqrt{\lambda}$ and $n_M = n_S\lambda^2$. This of course is not possible. As with many model test achieving absolute similitude is impossible, therefore, it is necessary to focus on the most important law for the given test. In the case of an open water propeller test, it has been found that Froude number can be ignore if certain conditions are met. A guideline established by the International Towing Tank Conference (ITTC) is to immerse the propeller to a depth of at least one and a half propeller diameters [2]. This guideline is to ensure the propeller does not draw air from the water surface. If this guideline is followed Froude scaling is not necessary.

In most test facilities it is not possible to achieve the same Reynolds number as the full-scale propeller. For this reason it is acceptable to conduct test at a lower Reynolds number as long as they are conducted in a turbulent region. Guidance from ITTC in 2002 states that "the propeller open water tests should be conducted at least at two Reynolds Numbers; one should be at the Reynolds Number used for the evaluation of the propulsion test and the other should be as high as possible" [3]. The ITTC subsequently recommended in 2014 to test at a Reynolds number no less

than 2×10^5 [2].

1.2   Open Water Propeller Testing

Open water propeller testing has been around for decades. Over the years researchers and laboratories around the world have collaborated through the ITTC to develop guidelines and procedures to conduct open water propeller tests. A typical open water propeller test boat is comprised of a few basic components; the body, propeller shaft, drive motor, thrust and torque sensor. The test boat is towed in a tow tank at various towing speeds and propeller speeds to achieve a rang of advance ratios. The test boat is towed with the propeller to the front providing a uniform inflow to the propeller. A four-quadrant test can also be conducted to test the propeller maneuvering performance, e.g. transitioning from ahead propulsion to astern. The four-quadrant test is conducted by towing the boat forward while spinning the propeller clock-wise and counter clock-wise then towing the boat backwards and spinning the propeller again in both directions.

1.3   Propeller Geometry

A standard marine propeller, or screw, is comprised of a number of blades which are fixed to a hub. The hub is a cylinder that typically tapers from front to back. The geometry of a marine propeller is commonly characterized by the following parameters.

Propeller diameter D. Twice the distance from the center of the hub to a single blade tip.

Hub diameter d. Twice the hub radius as defined in Figure **??**.

Propeller blade number Z.

Propeller pitch P.

Expanded area A_E. The surface area of the propeller equal to the area enclosed by an outline of a blade times Z.

Disk area A_O. The area of the circle swept out by the tips of the propeller blades.

These parameters are often nondimensionalized with the following ratios.

Pitch-diameter ratio P/D.
Expanded area ratio A_E/A_O.

The blades of a propeller are defined about the propeller reference line, a line norm to the shaft axis. Each propeller blade is formed by "stacking" cylindrical aerofoil sections along a generator line. These reference lines are illustrated in Figure 1-1.

The pitch of a propeller is the straight line distance traveled by the propeller in one revolution in a no-slip condition. This is best understood by imagining the propeller is a screw being drilled into wood; the pitch is the distance the screw travels in one rotation. As explained by the ITTC:

A helical path is generated by a point moving at a uniform velocity, V, along an axis while at the same time rotating about that axis at a uniform angular velocity, ω, at a distance, r, from the axis. The distance traveled along the axis in one revolution is called the pitch. [1]

1.4 Wageningen B-series

Among the most well known series of propellers is the B-series, a series of propellers designed and tested by the Netherlands Ship Model Basin in Wageningen. The B-series covers a range of different propellers with blades numbering from 2 to 7, expanded area ratios from 0.3 to 1.05, and pitch diameter ratios from 0.5 to 1.4. This series of propellers has been tested and analyzed extensively which has provided an excellent benchmark for propeller design. The open water performance curves of the B-series have been expressed as polynomials as a function of blade number, expanded area ratio, pitch-diameter ratio, and advance coefficient. These polynomials were developed through multiple polynomial regression analysis of 120 B-series models by

Oosterveld and Oosanen [4]. The results of this regression were used by Bernitsas, Ray, and Kinley to plot 96 open water propeller characteristics curves [5]. A similar approach was taken for this research by using these polynomials to make an Excel tool to generate open water curves for this range of B-series propellers.
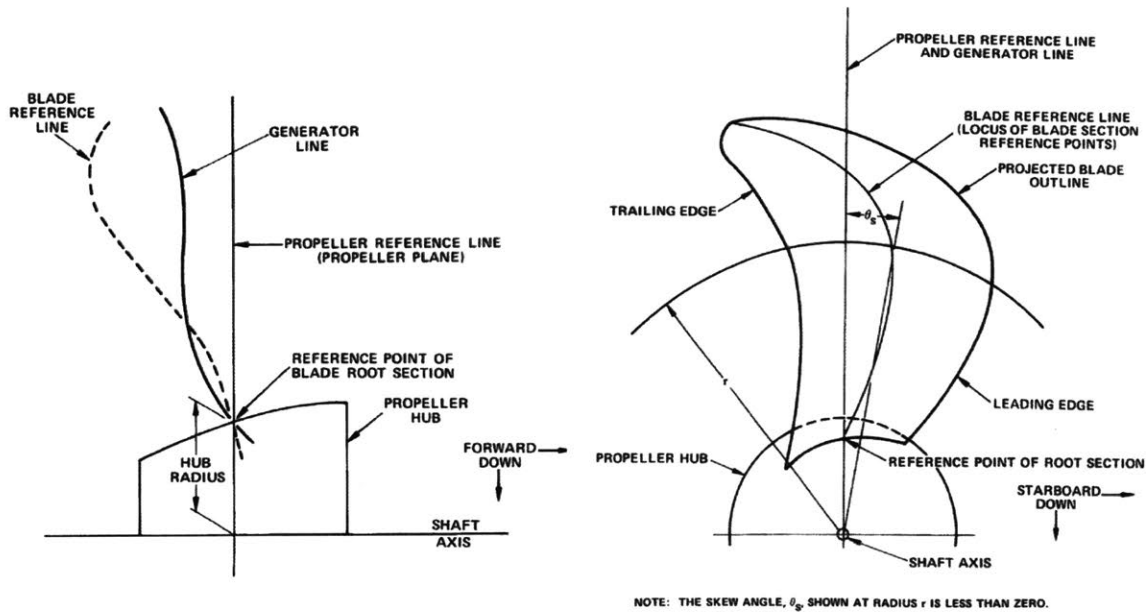
Figure 1-1: Propeller Reference Lines. *Figs. 2b & 2c ITTC - Recommended Procedures 7.5-01-02-01* [1]

1.5 Thesis Overview

This thesis is organized in the following manor. Chapter two begins by describing the design and construction of an open water propeller test boat. This chapter covers the design method and describes each component of the test boat. Chapter three covers the design and manufacturing of a 3D printed replica propeller. The capabilities and limitations of 3D printing a propeller using a benchtop SLA printer are discussed. An overview of the printing process and propeller assembly is given. Analysis of the replica propellers simulated open water performance, strength, geometrical accuracy, and surface roughness are also discussed. Chapter four describes the test setup and results. This chapter provides a comparison of the measured open water performance

to the expected performance of the benchmark and the replica propeller. Chapter five provides a discussion of the results. This discussion covers an overview of the results, factors of measurement uncertainty, and specific discussion of the discrepancies found during the benchmark and replica propeller testing. Finally, chapter six provides a conclusion to the project and offers recommendation for future work.

Chapter 2

Open Water Test Boat Design and Construction

2.1 Propeller Test Boat Design

The concept of a propeller test boat is relatively simple, but designing one that will provide accurate results is a challenge. The ITTC has developed design recommendations [2] for open water propeller testing that were used as a starting point for this design. Inspiration for this design was found from the multiple iterations of a test boat made by Webb Institute students [6] [7], and a boat designed to test super cavitating propellers made by Florida Atlantic students [8]. These examples and ITTC's recommendations [3] formed the foundation of this design.

A propeller test boat can be broken down to a few main components; a streamline body, propeller shaft, drive motor, thrust sensor, and torque sensor. When a single sensor is used to measure thrust and torque it is commonly referred to as a dynamometer. These basic components and their general arrangement are illustrated in figure 2-1. The sizing and arrangement of these basic components depend on different considerations including, but not limited to, cost, carriage capacity, sensor type, and propeller size. The numerous considerations made in this design will be discussed in the proceeding sections. These design considerations and constraints along with

the recommendations from the ITTC where constantly evaluated as the designed progressed.
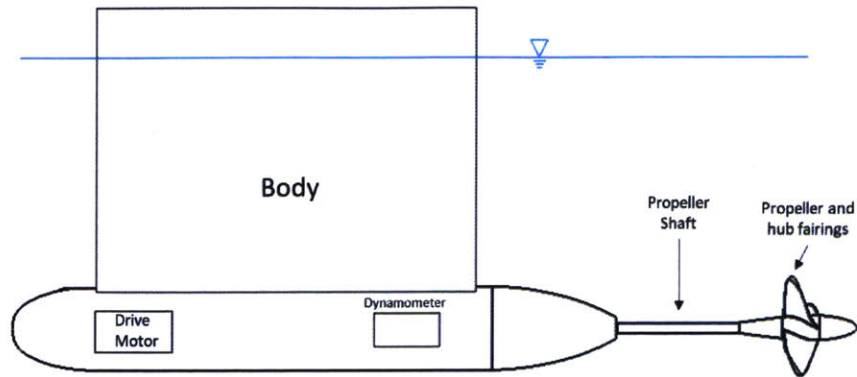
Figure 2-1: General open water propeller test boat layout

2.1.1 Design Process

A typical spiral design process was conducted to design the test boat. The spiral process is conducted in a sequential series of steps begins with the design requirements. At each step of the spiral a synthesis or analysis task is completed. This process is repeated until a balanced design is reached. The design spiral used for this project is illustrated in Figure 2-2.

The requirements for this design were defined by the ITTC - Recommended Procedures and Guidelines for Open Water Testing [2]. Additional requirements were derived from the limitations of the towing carriage and the tow tanks size. Table 2.1 lists the requirements for this project.

2.1.2 Design Considerations and Constraints

Testing facility: MIT's towing tank, a part of the Center for Ocean Engineering, was used to conduct these experiments. The towing tank dimensions are 15 m (49 ft) long by 2.4 m (8 ft) wide by 1.2 m (4 ft) deep. The length of 15 m is an effective length which is the range the towing carriage can travel. The depth is a max tank depth; typical water levels used for testing were approximately 40 inches. The tank
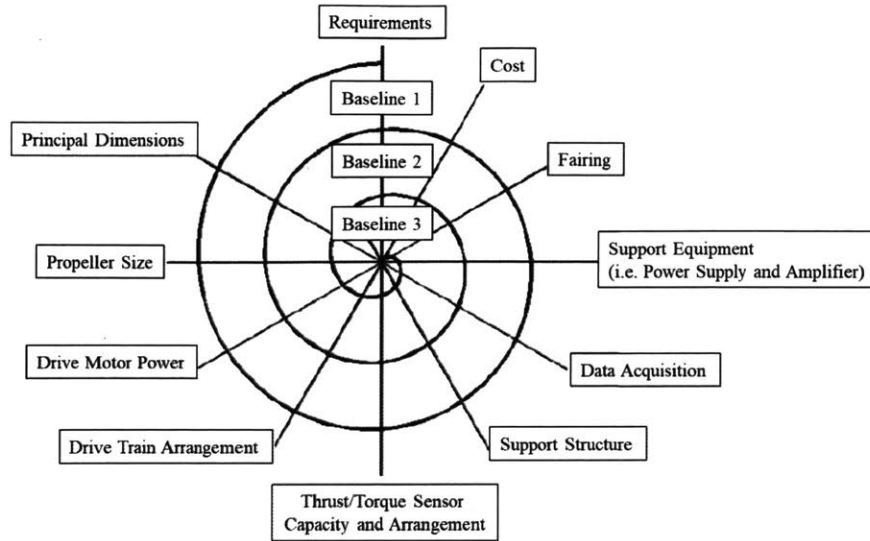
Figure 2-2: Open water propeller test boat design spiral.

Table 2.1: Design Requirements List.

Propeller Immersion Depth	Propeller should be immersed to at least 1.5 D, IAW ITTC
Propeller Shaft Length	Propeller should extend 1.5 to 2.0 D from drive shaft housing, IAW ITTC
Reynolds Number	At least 2×10^5 based on chord length at 0.7 R, IAW ITTC
Propeller Rate of Rotation	Must be constant throughout test run, IAW ITTC
Propeller Diameter	Estimated max of 0.229 m (9 in) based on tank size
Towing Speed	Max of 1.6 m/s (5.25 ft/s) due to limits of towing carriage

includes a beach at one end and a wave maker on the other. The carriage has a max towing speed of 2.4 m/s but for safety reasons (mostly safety of the equipment) the carriage was towed at a maximum of 1.6 m/s (5.25 ft/s).

Scale: A primary consideration for any model test is the scale of the model. In theory, it is most advantageous for the model to be as close to full-scale as possible. There are however practical limit that are quickly realized when determining the model size. The sizing of a model propeller is dependent on the test environment and the propeller boat capability.

As previously mentioned, both Froude and Reynolds laws must be considered

25

for propeller testing. Froude's law can be ignored if the propeller is immersed to a depth of 1.5 D. Taking this into consideration and the depth of the tank, an initial model propeller size of 9 inches in diameter was estimated. This size would allow the propeller to be sufficiently deep without being to close to the tank floor.

The primary consideration with respect to Reynolds law is to ensure the model propeller is tested in the turbulent region (or the operating region of the full-scale propeller). If the model propeller does not operate in the turbulent region, measured thrust and torque will be inaccurate when compared to full scale, thus making it more challenging to scale the model test results to full scale. The ITTC recommends a minimum Reynolds number of 2×10^5 [2]. The limiting factors are carriage capacity, drive motor power, thrust/torque sensor capacity, and the dimensions of the tow tank. The most direct way to increase Reynolds number is to increase the size of the propeller. However, increasing propeller diameter will quickly increase the amount of thrust and torque, with thrust increasing as D^4 and torque increase as D^5. A less restrictive way to increase Reynolds number is to increase propeller rotation, with thrust and torque increasing with n^2, while carefully considering to the limits of the propeller drive motor and carriage. As the propellers rate of rotation is increased the carriage speed must also be increased to achieve the required range of advance ratios. Advance ratios range from zero (max slip), to the point when the propellers pitch to diameter (P/D) ratio equals the advance ratio (no slip). Typical pitch to diameter ratios of marine propellers range from approximately 0.5 to 1.6.

Cost: This project had a limited budget which was a factor that drove the design. Having a limited budget meant the project would have to be completed by recycling pieces and parts from old projects. While not ideal, this approach lead to a tremendous amount of cost savings while still providing a capable test rig. The biggest drawback to this approach was not having all the required parts from the beginning. This ultimately resulted in a design that was not optimized to the sensor used to measure thrust, due to the fact that the sensor was changed late in the construction phase of the project.

2.1.3 Component Description

The final design of the propeller test boat is a chain driven, split thrust and torque sensor setup. The main body is a cylindrical aluminum manifold that support a stainless steel propeller shaft. The main body is fixed to the towing carriage with two aluminum struts. The drive motor is mounted on an aluminum skid above the main body. The propeller shaft is driven by the drive motor via a stainless steel drive shaft to a sprocket and chain. A three dimensional model of the final design was created in SOLIDWORKS 2017 and is illustrated in Figure 2-3. The final design assembly and bill of materials can be found in Appendix A.
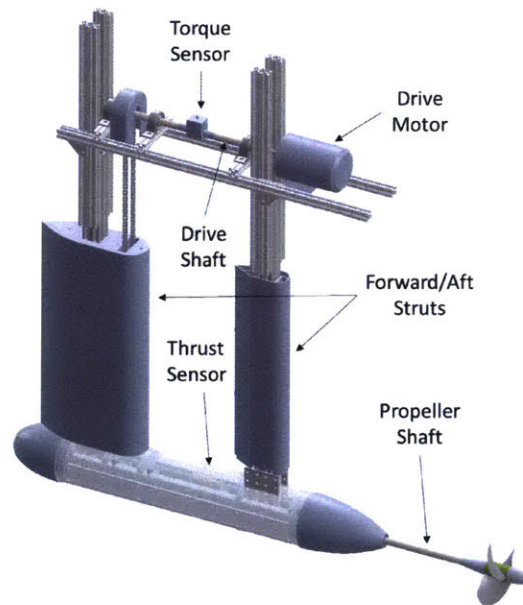
Figure 2-3: Propeller test boat final design 3D model.

Propeller Shaft Manifold: The design of the test boat is focused around the propeller shaft manifold. The propeller shaft manifold is made of five 0.5 inch aluminum plates bolted together with two 0.25 inch plates and two 1 x 1 inch 80/20 T-slot extrusions. The half inch plates house three stainless steel sealed ball bearings that support the propeller shaft. The 80/20 T-slot framing provides a mounting point for the 2 x 2 inch 80/20 T-slot struts. The struts are mounted to the manifold with a

double flange linear bearing which allows the manifold to slide on and off the struts. A 1/8 inch thick clear polycarbonate tube encases the exterior of the manifold. All fasteners used to bolt the manifold together are 1/4"-20. A three dimensional drawing of the manifold can be seen in Figure 2-4.
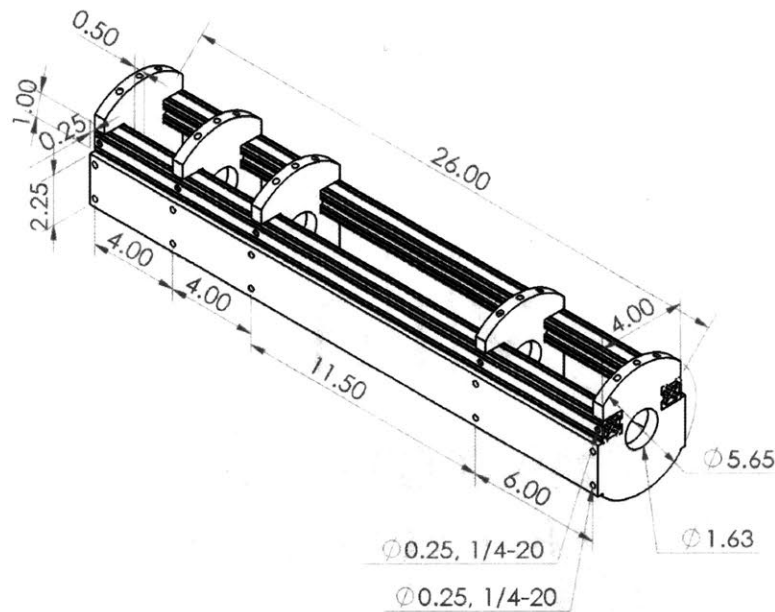
Figure 2-4: Propeller shaft manifold model

Thrust Sensor: The sensor used to measure thrust is an AMTI (Advanced Mechanical Technology, Incorporated) MC1-6-250. This sensor is a water proof strain gauge type sensor designed to measure forces and moments. The sensor measures three orthogonal force components along the X, Y, and Z axes and the moments about those axes. The sensors specifications can be found in Appendix B. The manufacture provides values of calibrated sensitivity are provided in Appendix C. From these sensitivities a load in any direction can be calculated with the following equation.

$$F_f = \frac{V_{fout}}{V_{fexc} * S_f * G_f * 1x10^-6} \qquad (2.1)$$

Where

F_f is the load in the f direction in pounds or Newtons

28

V_{fout} is the amplified voltage output for the f channel in volts

V_{fexc} is the excitation voltage applied to the bridge in volts

G_f is the amplifier gain

S_f is the calibrated gain sensitivity in $microVolts/V_{exc-lb}$ or $microVolts/V_{exc-N}$

The output voltage of the MC1 sensor is amplified with an AMTI MSA-6 MiniAmp. The MSA-6 is a six channel strain gauge amplifier design for sensors like the MC1. The gain and excitation of each channel is manually set with jumpers. The amplifiers analoge output signal is rated to +/- 10 VDC.

The thrust sensor is mounted to the propeller shaft via a double flanged stainless steel roller bearing. The sensor is mounted parallel to the propeller shaft and bolted to the bearing flange as depicted in Figure 2-5. The opposite flange is mounted to a rigid cross-member in a similar fashion. In this configuration the resultant force measured is half of the total axial force exerted on the propeller shaft.
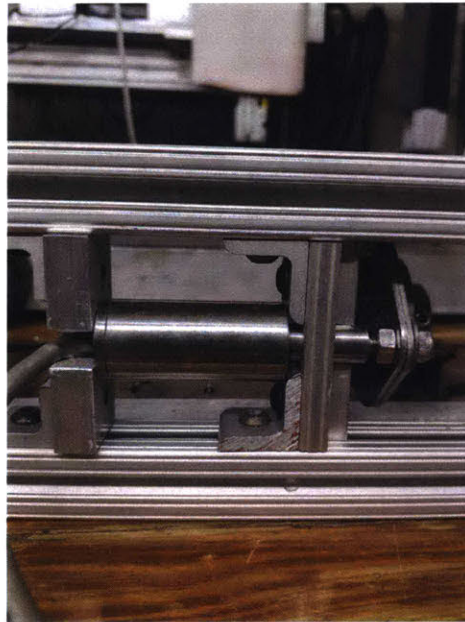
Figure 2-5: Thrust sensor mounting configuration

Torque Sensor: The sensor used to measure torque is a Futek TRS600. The TRS600 is a non-contact rotary torque strain gauge sensor. This torque sensor has a maximum capacity of 20 N-m in both the clockwise and counterclockwise direction. The sensor

specification can be found in Appendix D. Calibrating data from the manufacturer can be seen in Appendix C. The torque sensor is mounted in-line with the drive shaft between the drive motor and sprocket. The analog voltage output of the sensor has a linear relationship to measured torque as expressed in equations 2.2 and 2.3. An excitation voltage of 11-26 VDC is supplied and an output of +/- 5 VDC is returned.

$$Q_{cw} = -4.0125 * Volts \qquad (2.2)$$

$$Q_{ccw} = 4.0055 * Volts \qquad (2.3)$$

Motor and Driver: The drive motor is a Bodine Electric Company 42R, inverter duty, 3/8 hp, A/C motor. This motor generates a max torque of just under 2 N-m at 1,455 RPM. The motor is driven by a Pacesetter adjustable speed motor driver. The motor driver uses a pulse width modulated (PWM) signal to control the motor speed. The driver frequency can be manually adjusted from 0 to 140 Hz, resulting in a max motor speed of 3500 RPM.

Tachometer: A switch Hall effect sensor is used as a tachometer. The Hall effect sensors voltage output is varied by a magnetic field, which is a convenient and inexpensive way to create a non-contact tachometer by coupling the sensor with a magnet. A magnet was mounted to the drive shaft and the sensor was mounted just above the magnet. With each shaft rotation the magnet passes the sensor creating a voltage pulse. These pulses are then used to measure the shafts RPM.

Drive Train: Beginning from the drive motor, a 0.75 inch diameter stainless steel shaft is coupled to the motor with a flexible coupling. The drive shaft is supported with three stainless steel mounted ball bearings. A steel ANSI number 35 sprocket is mounted to the drive shaft and connected to the propeller shaft with a 3/8 inch steel chain. The propeller shaft is mounted in the propeller shaft manifold with three stainless steel sealed ball bearings. The propeller shaft exits the manifold into the nose cone where it is supported with an oil-embedded bronze sleeve bearing. The end

30

of the propeller shaft is threaded to 3/8"-16 by 2.75 inches long and a 0.5 x 0.5 inch square flat is machined into the shaft at the base of the threads.

Nose Cone: The nose cone is machined from a polymer material called Delrin. The nose cone is 8.75 inches long and the base is 5.95 inches in diameter and tappers down to 1.5 inches at the end. The nose cone serves two purposes; the first is to add support to the propeller shaft as close to the propeller as possible. This arrangement helps to eliminate shaft wobble. The second purpose is to reduce pressure build up as the boat is towed through the water. The ITTC recommends a distance of 1.5 to 2 propeller diameters from the propeller blades to the housing [2]. The distance from the end of the nose cone to the base of the propeller hub is 11.75 inches.

Strut Fairings: The primary purpose of the strut fairings is to reduce the wake and bow wave that is generated when the boat is towed through the water. The struts are foil-like shapes with a rounded nose and pointed tail. The fairings slide over the 80/20 struts and extend from the propeller shaft manifold to a few inches above the waterline. The forward strut dimensions are 6.25 in L x 2.5 in W x 22.5 in H. The forward strut is 3D printed in three sections from ABS plastic filament. The aft strut dimensions are 12 in L x 4 in W x 24 in H. The aft strut was machined from urethane foam and covered in Bondo® body filler.

Data Acquisition Hardware: The analog voltage outputs from the thrust, torque, and Hall effect sensors are collected by a National Instruments (NI) USB-6211 data acquisition (DAQ) device. The DAQ takes the analog voltage and converts it into a digital signal that is transmitted through USB to a computer. The DAQ was also used to supply analog output signals that are used to control the motor driver. A complete wiring schematic can be seen in Appendix E.

THIS PAGE INTENTIONALLY LEFT BLANK

Chapter 3

Replica Propeller Design and Manufacturing

3.1 Benchmark Propeller

The benchmark propeller used to validate the performance of the test boat was an aluminum Wageningen B3-70 model. This propeller was borrowed from the Naval Surface Warfare Center Carderock (NSWCC) and its model number is 4276. The dimension of the model propeller are provided in Table 3.1.

Table 3.1: Benchmark Model Propeller Principle Dimensions.

NSWCC Propeller Model 4276 (Wageningen B3-70)	
D (in)	7.623
No. Blades	3
Pitch (in)	8.156
P/D	1.07
Ae/Ao	0.7
Hub dia. B (in)	1.75
Hub dia. F (in)	1.524
Hub Length (in)	2.7

The open water performance of model 4276 was measured by NSWCC and is provide in Appendix F.

3.2   3D Printed Propeller Replica

A 3D printed replica, similar to the benchmark propeller, was manufactured using a Formlabs Form 2 Stereolithography (SLA) 3D printer. The Form 2 printer was provided by the Laboratory for Manufacturing and Production at MIT which utilizes multiple Form 2 printers for classes and research. The Form 2 is a benchtop 3D printer that uses SLA technology to create polymer parts from resin. Stereolithography is a process used to print 3D parts in a layer by layer processing using an ultraviolet laser to harden each layer.

3.2.1   3D Printed Propeller Considerations

Additive manufacturing machines such as the Form 2 provide a user-friendly and simple way to quickly manufacture nearly anything the user can model in 3D. There are however some limitations to 3D printing, the size of a single print being the primary limitation. The capabilities of a 3D printer must be taken into account when factors such as strength and precision are important. The primary factors that were considered when printing the replica propeller were geometrical accuracy, blade strength, and surface finish.

The geometrical accuracy required for a model propeller as defined by the ITTC [9] are extremely stringent. All dimensions of the model propeller, i.e. diameter, pitch, and section shape, must not vary more than a fraction of a percent. A 3D printers precision is a function of a few factors, the primary factor being the resolution (also referred to as step size). The resolution of a 3D printer is simply the layer height. The layer height is extremely important, especially when printing small parts with features that approach the layer height. The resolution also determines the surface finish. A propeller must not only have a smooth surface, it must have a thin and sharp trailing edge. When comparing 3D printers, a typical Fused Deposition Modeling (FDM) printer can have resolutions as small as 100 microns and SLA printers can achieve resolutions as small as 25 microns.

A variety of materials can be used for 3D printing. The material selected will

determine the parts strength and other properties. When printing a propeller it is import to considered the rigidity, water absorption characteristics, and machine-ability of the material. Model propeller blades are thin and can flex during testing if the printed propeller is not rigid enough. The rigidity and strength of a printed part is unique to each 3D printer and is dependent on the material, print orientation, and resolution. The porosity of a printed part can lead to water absorption causing the part to swell and deform. Most 3D prints require post-processing to remove support material and potentially refine the shape. Some parts may be too large to print as one piece and must be printed in multiple pieces and fastened together. For a model propeller it may be necessary to sand or machine the blades to achieve the necessary geometrical accuracy and surface finish.

3.2.2 Form 2 Printer Capabilities and Limitations

The Form 2 is a user friendly printer that utilizes an intuitive software called Pre-Form that makes the printing process extremely simple. The Form 2 printer provides resolutions of 25, 50, and 100 microns. The small resolution of the Form 2 provide a high degree of geometrical accuracy and an excellent surface finish. Formlabs offers many different types of resins, each formulated to achieve desirable engineering properties such as toughness and durability. The printing volume of the printer is somewhat limited but comparable to most desktop printers. The Form 2's build volume is 145 X 145 X 175 mm or 5.7 X 5.7 X 6.9 inches.

Through research and some trial and error a few important considerations were made when printing a model propeller with the Form 2. The first considerations is the amount of support structure. Before the Form 2 prints it generates support structure around the part. This support structure is necessary to provide a foundation for the part and to prevent the part from deforming. When printing a propeller there is a delicate balance between too much and too little support structure. Too much structure can effect the shape of the propeller blade and will require additional post-processing. Too little support structure will commonly lead to pieces of the part breaking and sticking to the bottom of the resin tank. Figure 3-1 is an example of a

properly oriented propeller after support structure has been added.
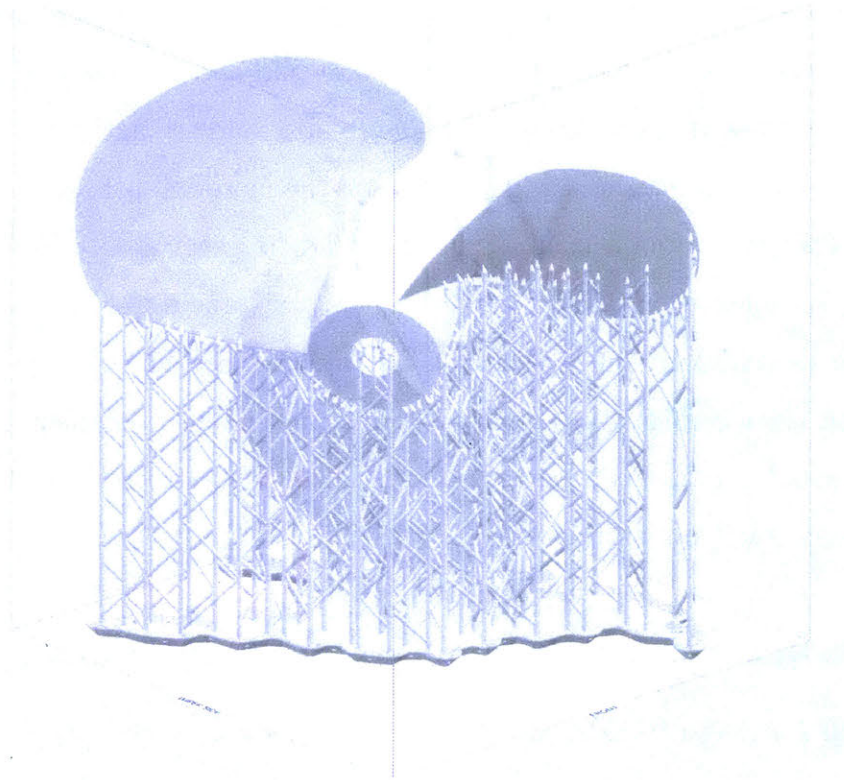
Figure 3-1: Example of Form 2 print orientation and support structure. Image captured from Formlabs Preform software.

The second consideration is the touchpoint size. The touchpoint size refers to the point where the support structure contacts the part. Again, there is a delicate balance between having too large or too small of a touchpoint. Too small of a touchpoint can lead to inadequate support and print failure. Too large of a touchpoint can be difficult to remove and could cause damage to the part during the removal process.

These first two consideration can typically be overcome by allowing the Preform software to generate the necessary support and choosing the default touchpoint size. However, for a propeller, some modification are necessary. When the Preform software generates the supports it places them on the parts edge and in the case of a propeller this mean on the blades edge. This creates issues especially on the trailing edge because the trailing edge is typically thinner than the touchpoint. If the support structure is printed on the blades edge it will take small chips out of the blade. To overcome this issue the support structure must be manually adjusted. The best

36

practice is to manually relocate the support structure just off the edge and stagger the support structure on either side of the edge. It is best to keep the density of support structure as close to what was originally generated by Preform as possible. Even with this modification there is a risk of damaging the blades edge when removing the support structure. To reduce this risk the touchpoint size was reduced to 0.7 mm.

The final consideration was the propeller orientation. After each layer of the part is printed the resin tank shifts laterally to remove the part from the resin tank bottom. This process has the potential to damage a print if it is not oriented properly or does not have adequate support. The Preform software will automatically orient the part so that the part will build off of itself and therefore minimize the risk of the part shearing off onto the resin tank. For a propeller there is not an orientation that is optimal for every blade, especially an odd number of blades. For this reason it is best to print one blade at a time or to change the orientation to a position that is optimal for as many blades as possible. The author found that the best orientation of a single blade is to have the blade build off the hub and leading edge. The part should also be angled slightly so the hub is not sitting flat on the build platform. The blade should be oriented, as close as possible, to have the blade aligned opposite to the resin tank motion with the leading edge forward. Figure 3-2 illustrates how a single blade was prepared for printing in the preform software.

3.2.3   Replica 3D Model

The ideal approach to replicating the benchmark propeller would have been to start from an exact 3D model generated from a 3D scan of the propeller. Unfortunately, an accurate 3D scan of the propeller could not be made with the scanner used by the author and outsourcing this work would have been too costly. The benchmark propeller was manufactured in the late 1960's and a 3D model was not available from NSWCC. For this reason a Wageningen B3-70 model was created using a free online tool [1]. The tool can either generate an optimizes B-series propeller based on user

---

[1]The free online B-series propeller generator can be found at, www.wageningen-B-series-propeller.com. The online B-series propeller generator is provided by FRIENDSHIP SYSTEMS
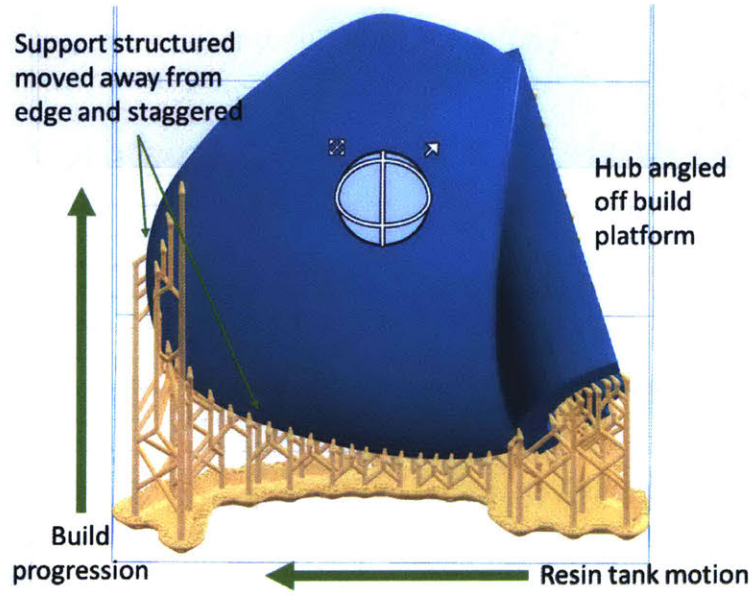
Figure 3-2: Example of a single blade print orientation and support structure.

input in the form of ship and propulsion parameters, or the user can input geome-
try parameters (such as diameter and pitch) to generate a specific B-series propeller.
The 3D model is generated by CASES® a 3D modeling software. Once the propeller
model is generated it can be saved as a STEP-File which can be opened and edited in
many different CAD programs. The replica 3D model was generated by inputting the
dimension of the full-scale propeller that the benchmark 4276 propeller was modeled
after. The dimensions of the full-scale B3-70 propeller are provided in Table 3.2. The
model generated from these dimensions was then imported into SOLIDWORKS and
scaled down to model size.

After the 3D model was generated the dimensions of the propeller were verified.
All principle dimensions, diameter, P/D, A_E/A_O, and hub dimensions, were exactly as
specified. The cylindrical sections of the model blades were also measured. The chord
lengths and max section thickness' were measured and compared to the expected
values of a Wageningen B3-70 with a diameter of 7.623 in and a P/D of 1.07. The
results of this comparison are shown in Table 3.3. As can be seen, the chord lengths

---

and was developed in collaboration with ISA Propulsion.

Table 3.2: Model 4276 Full-scale Propeller Dimensions.

Full-scale Geometry of NSWCC Propeller Model 4276 (Wageningen B3-70)	
D (in)	240
No. Blades	3
P/D	1.07
Ae/Ao	0.7
Hub dia. B (in)	55.097
Hub dia. F (in)	47.98
Hub Length (in)	85
Root Thickness (in)	9.75
Tip Thickness (in)	0.72

of each section were nearly exact with the exception of the section at 0.7R. Overall the replica model blades are slightly thicker than expected.

Table 3.3: Cylindrical Section Chord and Thickness Comparison.

Section	Replica 3D Model		B-series		Difference	
	Chord	Max t (in)	Chord (in)	Max t (in)	Chord (in)	Max t (in)
0.4R	3.554	0.245	3.557	0.238	-0.003	0.007
0.5R	3.769	0.215	3.771	0.202	-0.002	0.013
0.6R	3.888	0.184	3.888	0.166	0.000	0.018
0.7R	3.914	0.154	3.856	0.130	0.058	0.024
0.8R	3.784	0.124	3.783	0.095	0.001	0.029
0.9R	2.95	0.094	2.947	0.059	0.003	0.035

3.2.4 Replica 3D Model CFD Analysis and Open Water Performance

A computational fluid dynamics (CFD) analysis was conducted to simulate the open water performance of the replica 3D model using the open source software OpenFOAM. The analysis was conducted in collaboration with Ioannis Dagres [10]. OpenFOAM was used to conduct a Reynolds-averaged Navier-Stokes (RANS) analysis of the propeller model. This analysis simulated the open water performance of the propeller under the same condition as the actual test. The results of this simulations are provided in Table 3.4. The results of this simulation closely agree with the

Table 3.4: Replica Model CFD Open Water Simulation Results.

OpenFOAM RANS CFD Results				
Wageningen B3-70 Replica 3D Model				
J	T (N)	Q (N-m)	KT	10KQ
0.1	46.77	1.41	0.48	0.75
0.3	38.80	1.19	0.40	0.63
0.5	29.27	0.93	0.30	0.49
0.7	19.63	0.67	0.20	0.36
0.9	10.85	0.42	0.11	0.22

expected open water performance of a Wageningen B3-70 and the performance data given for model 4276. A comparison of these results can be seen in Figure 3-3.
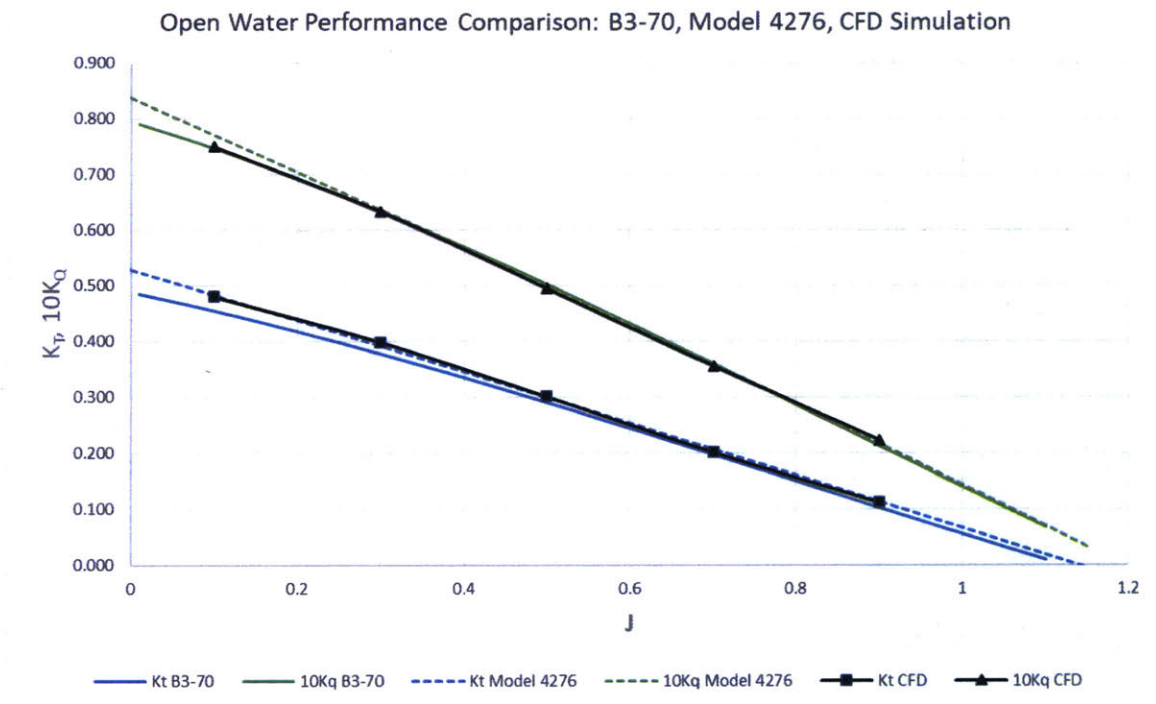
Figure 3-3: K_T and $10K_Q$ curves of B3-70, model 4276, and CFD results of replica model.

3.2.5 Replica 3D Model Strength Analysis

Further analysis and simulation of the replica models strength was conducted by Dagres [10]. The pressure distribution field developed in the Openfoam simulation

was exported into an Autodesk FEA (Finite Element Analysis) program to analyses the stress and deflection of the propeller blades. A tension modulus of 2.8 GPa and a Poisson ratio of 0.33 were used for this analysis. These material properties were provide by the manufacture for a part printed at a resolution of 100 microns and cured for one hour. The results of this analysis show a maximum stress occurring at the blade root of 1.08 MPa which is much less than the ultimate strength of 58.3 MPa. The resulting deflection of the blades was virtually zero ($0.19e^{-6}$ mm at the blade tip).

3.2.6 Propeller Construction

The propeller was printed from Formlabs "High Temp" resin at a resolution of 50 microns. After each print the part was rinsed in a solvent bath and cured in a Formlabs curing oven. Because the model propeller was too large to print as one part, each blade had to be printed separately and then epoxied together. A model of one blade was created from the scaled propeller model by slicing it like a pie and taking a 120 degree section. Two aluminum rings were embedded on either end of the hub as a base to assemble the blade while ensuring each blade aligned properly. The aluminum rings also acted as a mounting point for two 5-40 bolts. These bolts where used to secure the propeller in a vice for machining. Small studs and holes were also added to the model to ensure each blade was properly aligned. Figure 3-4 illustrates how the model propeller was assembled.

After the propeller was assembled and epoxied the hub hole was drilled to its final diameter of 0.5". Each hub face was then milled and sanded to removed excess epoxy and material to ensure the hub face was completely flat and perpendicular to the hub hole. The propellers surface was then sanded smooth and painted. The surfaces were smoothed by first filing down any excess support material and then the entire propeller was sanded with 400 grit sandpaper. Two layers of epoxy spray paint were then added. The first layer of paint was added and then wet sanded with 800 grit sandpaper before adding the second and final layer of paint. Finally, a small beveled grooved was filed into the back of the hub to be mated to the beveled point in the
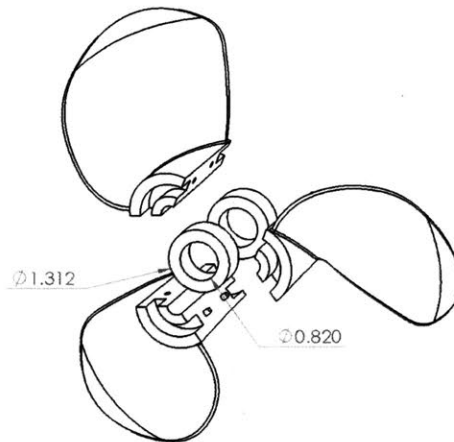
Figure 3-4: Assembly of model propeller blades and hub rings.

aft fairing.

3.3   Replica Propeller As-built Characteristics

To accurately represent the actual replica propeller the as-built characteristics of the propeller were evaluated. Some observations were made during the construction process that indicated areas of concerns. The first and most concerning was a mis-alignment of the blades when they were mounted to the hub rings. This mis-alignment was caused by a deflection of the hub outward from front to back as shown in Figure 3-5. It is not clear what caused the part to print this way. A potential cause could be the lack of support material in this area.

A second concern was triangular pattern in the parts surface. This pattern is a result of the STL format. An STL model is a recreated model of triangulated surfaces. This triangular pattern becomes apparent particularly in the drastically curved potions of the part, such as the blade root and the hub. As a result these portions of the propeller required additional sanding.
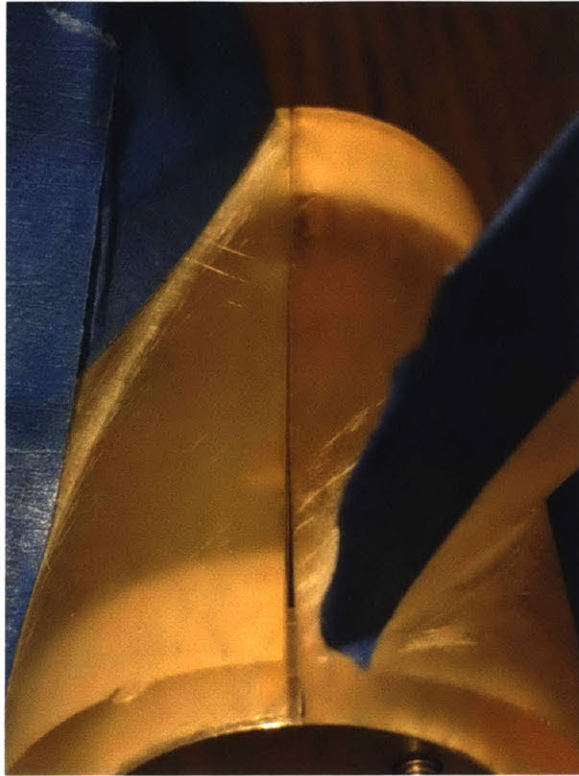
Figure 3-5: Image of hub deflection observed during propeller construction.

3.3.1 Geometry

The overall dimensions of the replica propeller were measured and are presented in Table 3.5. Measurements were taken manually using a milling machine. The milling machines was used as a coordinate measuring device by placing a deflection gauge in the tool chuck to measure the x, y, and z coordinate. To recreate a 3D model of the as-built replica, coordinates were mapped to the surface of the propeller hub and one blade face. A total of one hundred coordinates were take to generate a point cloud that was then imported into Rhinoceros 5 (a 3D CAD program). The recreated model was then compared to the replica 3D model as shown in Figure 3-6.

As seen from this comparison the as-built replica does not match the replica model exactly. The blade follows a similar contour but each blade has been rotated slightly. This slight rotation of the blade resulted in an increase in pitch and decrease in the expanded area ratio.

Table 3.5: As-built Replica Propeller Principle Dimensions.

Replica Propeller (As-built)	
D (in)	7.571
No. Blades	3
Pitch (in)	8.646
P/D	1.14
Ae/Ao	0.68
Hub dia. B (in)	1.78
Hub dia. F (in)	1.517
Hub Length (in)	2.68

Figure 3-6: 3D comparison of as-built replica and replica 3D model. Green is recreated model and grey is original model. Left: 3D recreation of as-built replica with point cloud. Right: as-built model overlaid on original replica model.

3.3.2 Surface Roughness

The surface of a model propeller must be hydrodynamically smooth and free of surface blemishes. The ITTC recommends a mean surface roughness of 0.3 to 0.5 μm [9]. To ensure the replica propellers surface was within this range the surface roughness of four printed samples was measured with a Bruker DXT Stylus Profilometer. The four samples were prepared in increments just as the replica propellers surfaces was smoothed, from no smoothing to smoothed and painted. The first samples was not smooth, the second was lightly filed, the third was filed and sanded, the fourth was filed, sanded, and painted. Each samples surface roughness was measured in accordance with ISO 4287. The results of these measurements are provided in Table 3.6.

Table 3.6: Surface Roughness Measurement Results.

Surface Roughness Measurements				
Sample	1	2	3	4
Parameter	Value	Value	Value	Value
Ra	1.299 μm	0.899 μm	0.243 μm	0.176 μm
Rq	1.485 μm	1.246 μm	0.295 μm	0.229 μm
Rsk	-0.076	-0.414	-0.021	1.195
Rku	1.757	2.8	2.173	4.182
Rz	4.404 μm	5.476 μm	1.162 μm	1.090 μm
Rp	2.233 μm	2.161 μm	0.533 μm	0.723 μm
Rv	2.170 μm	3.315 μm	0.629 μm	0.366 μm
Rt	7.448 μm	5.798 μm	1.274 μm	1.090 μm

The results of these measurements show the smoothing process achieved an exceptionally smooth surface, in fact the roughness of the fourth sample was just below the recommended range.

THIS PAGE INTENTIONALLY LEFT BLANK

Chapter 4

Testing and Data Analysis

4.1 Test Preparation

Prior to any testing, preparations were made to ensure accurate and useful data was collected. A data acquisition system and process was established to ensure data was properly collected and stored. Each sensor was also tested and calibrated.

4.1.1 Data Collection

MATLAB was used to record, view, and process the data acquired from the propeller boat sensors. A MATLAB script was written to collect and store the data acquired by the DAQ in a comma separated value (CSV) format. A graphical user interface (GUI) was also created with this script that plotted the filtered sensor data in real time. Included in the GUI was a run/stop button that controlled the analog voltage output to the motor driver, thus remotely turning the motor on and off. This script allowed a single user to run an entire experiment from one computer. The MATLAB script was run from a laptop that was mounted on the towing carriage in proximity to the test boat. This laptop was then operated remotely from a desktop computer used to run the towing carriage.

4.1.2 Sensor Calibration

Torque Sensor: The torque sensor was calibrated by the manufacturer and did not require in situ calibration. To measure the torque generated by the propeller the torque added by the system must be eliminated from the torque of the propeller, essentially conducting a dynamic tare of the sensor. This process was done by first measuring the torque of the propeller boat with a dummy hub. A dummy hub is a blade-less propeller with the same dimensions of the propeller hub and equal in weight to the propeller. These torque measurement were taken over a range of RPM's to establish the systems torque as a function of RPM.

Thrust Sensor: Since the thrust sensor is relatively old and had been used previously, its calibration was checked using the calibrations data provided by the manufacture. The MC1 sensor was used in at least three different projects from 2004 to 2008. The last known "in-house" calibration of the MC1 was conducted by Lim [11] in 2005. Lim's calibration resulted in close agreement with the manufactures calibration. To verify the sensor was still in calibration a simple test of the z-axis sensitivity was conducted using graduated weights. The results of this test were also in close agreement with the manufactures calibrated sensitivity. The MC1 users manual was also consulted to determine calibration periodicity. AMTI states the MC1 does not require calibrations as long as the sensor is operated in the elastic region and not subject to damage or gross overloads. With this information it was decided that the sensor was within calibration.

Prior to testing, the MC1 sensor and amplifier were energized for a least one hour per AMTI's recommendation. This time allows the sensor to reach thermal equilibrium. A static in situ calibration of the MC1 was conducted with graduated weights and a rope and pulley system. Weights were hung from a rope and pulley system that would then pull on the end of the shaft. This calibration confirmed the thrust sensor was accurately measuring half of the resulted axial force applied to the shaft. The MC1 sensor is extremely sensitive and even the smallest amount of displacement of the propeller shaft will result in a notable amount of force. This

sensitivity results in noise in the thrust data as the shaft spins. The shafts starting position also varies from run to run. For this reason a dynamic zero was established. To establish the dynamic zero the thrust of the propeller in a bollard condition ($V_a = 0$) was measured over a range of shaft RPM. To begin these measurement the thrust sensor is zeroed by the amplifier and the position of the drive shaft is marked. Between each measurement the shaft is reset to the zero position.

4.1.3 Test Procedure

Prior to each test a series of motor drive frequencies and carriage speeds were set to ensure testing was conducted over a sufficient range of advance ratios. The following procedures where then followed.

- Measure and record water temperature.

- Install dummy hub and propeller hub fairings.

- Mount test boat to towing carriage and wire components according to Figure E-1.

- Energize equipment and test drive motor.

- Run MATLAB script, initialize DAQ, and test functionality.

- Establish remote connection to laptop from carriage control desktop computer.

- Test carriage function.

- Ensure at least one hour has elapsed before taking measurements.

- Conduct dummy hub measurements over RPM range of the test.

- Measure drag of hub over range of test towing speeds.

- Install propeller and conduct bollard thrust measurements.

- Conduct tests at advance ratios from $J = 0$ until $K_T < 0$. Allow tank to settle between each run.

4.2 Benchmark Propeller Testing and Results

The benchmark propeller was tested over a range of RPMs. Two runs were conducted at six different carriage speeds and five different motor driver frequencies for a total of 60 runs. Since the propeller RPM could not be actively controlled, a range of motor driver frequencies were used to vary the propeller RPM. Propeller RPM was then a function of driver frequency and carriage speed. The actual propeller RPM was later measured when the data was processed. The motor driver frequencies were set to 20, 22, 24, 26, and 28 Hz and carriage speeds set to 0.25, 0.5, 0.75, 1, 1.3, and 1.6 m/s. This testing approach covered a range of advance ratios from approximately 0.15 to 1. The average Reynolds number of all 60 runs was 1.62×10^5.

4.2.1 Dummy Hub Measurements

Torque measurements using the dummy hub were taken at motor driver frequencies of 18, 22(twice), 24, 26, and 28 Hz. The measured torque was plotted against RPM and a line was fit to the data.

Benchmark Propeller Tare Torque

$$y = 0.00016x + 0.40752$$
$$R^2 = 0.90380$$
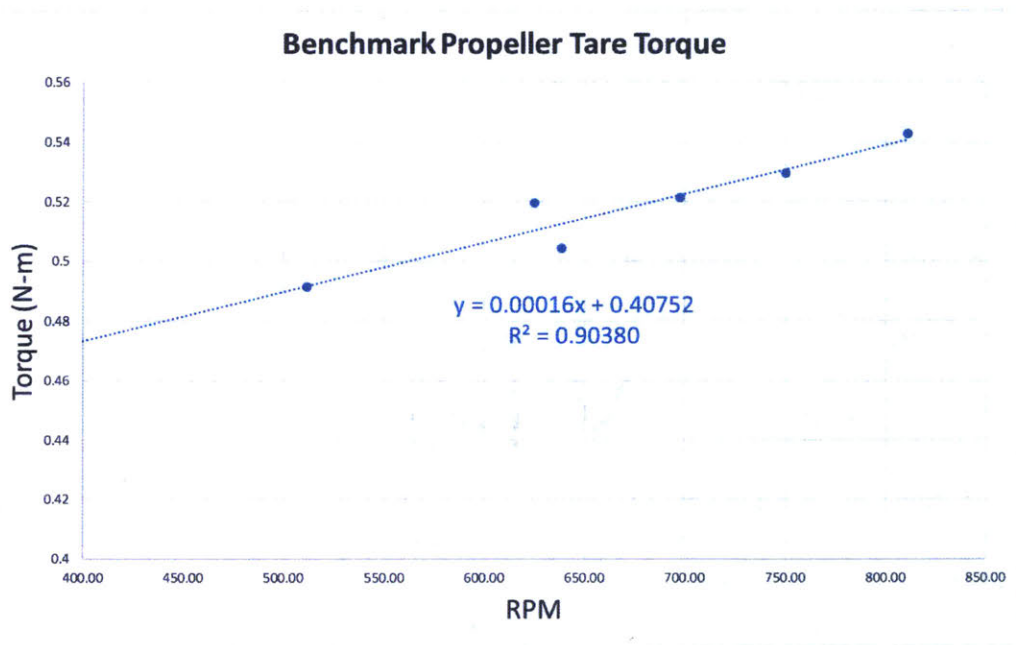
Figure 4-1: Benchmark dummy hub torque measurements.

Based on these measurements the following equation was used to zero the torque

measurements.

$$Q_{tare} = 0.0001646 * RPM + 0.4075 \tag{4.1}$$

Although this equation does not equal zero when RPM is zero, it was assumed the relationship between torque and RPM is linear over this range of RPM.

4.2.2   Hub Drag Measurements

Precise measurement of the propeller hubs drag proved to be difficult and measurements tended to be significantly different than expected. For this reason, hub drag was accounted for by bluff body approximation using equation 4.2.

$$Drag = C_D * S * (1/2 * \rho * U^2) \tag{4.2}$$

Where, C_D is the drag coefficient, S is the projected area, and U is velocity. A value of 0.5 was used for the coefficient of drag C_D. This value is the coefficient of drag for a sphere in laminar flow.

4.2.3   Bollard Measurements

Bollard measurements were taken at driver frequencies from 18 to 28 Hz in 2 Hz increments. The measurements taken at 22 and 26 Hz were determined to be inaccurate and removed from the data set. The measured thrust values where plotted against RPM and a power trend line was fit to the data. The theoretical values of thrust were also plotted and compared to the measured values. Figure 4-2 is a plot of the measured and theoretical bollard thrust values.

The following equations was used to calculate expected bollard thrust for each run.

$$T_b = 0.0001079 * RPM^{2.0816} \tag{4.3}$$

The measured values of thrust do not increase with RPM squared as theory states. This deviation from theory and the slightly lower values of measured thrust are likely due to binding in the nose cone.

Benchmark Propeller Bollard Test

$y = 0.00021x^{2.00000}$
$R^2 = 1.00000$

$y = 0.00011x^{2.08156}$
$R^2 = 0.99116$
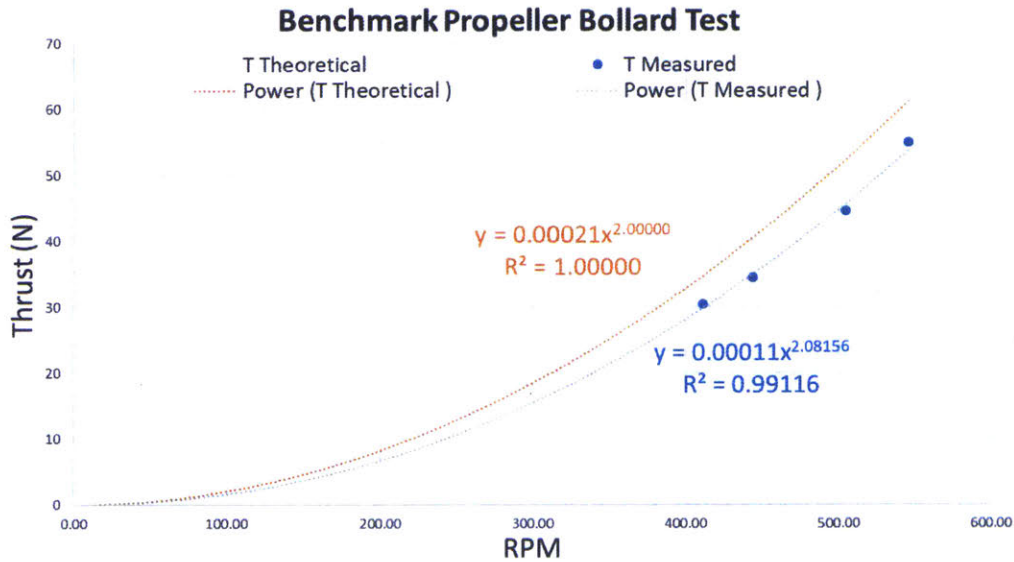
Figure 4-2: Benchmark bollard thrust measurements.

4.2.4 Open Water Performance

After all 60 runs were conducted the data was analyzed using MATLAB. The sampling rate of each run was set at 500 samples/sec. The raw data was filtered with a low pass Butterworth filter with normalized pass and stop band frequencies of 0.001 (0.25 Hz) and 0.5 (125 Hz) respectively, a pass band ripple of 1 dB, and a stop band attenuation of 60 dB was also specified. The filtered data was then plotted and the range over which the data was to be averaged was selected. Figure 4-3 is an example of filtered thrust and torque voltage values of a typical run.

It should be noted when reading Figure 4-3 that negative voltage corresponds to positive torque and thrust. It is clear to see from this plot the process of the run. The first decrease in voltage is when the propeller shaft begins to spin, the next increase in voltage is when the carriage starts, followed by another decrease when the carriage stops, and finally both voltage readings return to nearly zero when the propeller shaft stops. For each run the average bollard voltage was taking over the first few second after the propeller shaft started to spin. An average voltage was taken for each run once the carriage and test boat reached a steady state. Steady state was reach at different times for different carriage speeds. Not only did the carriage have to reach a
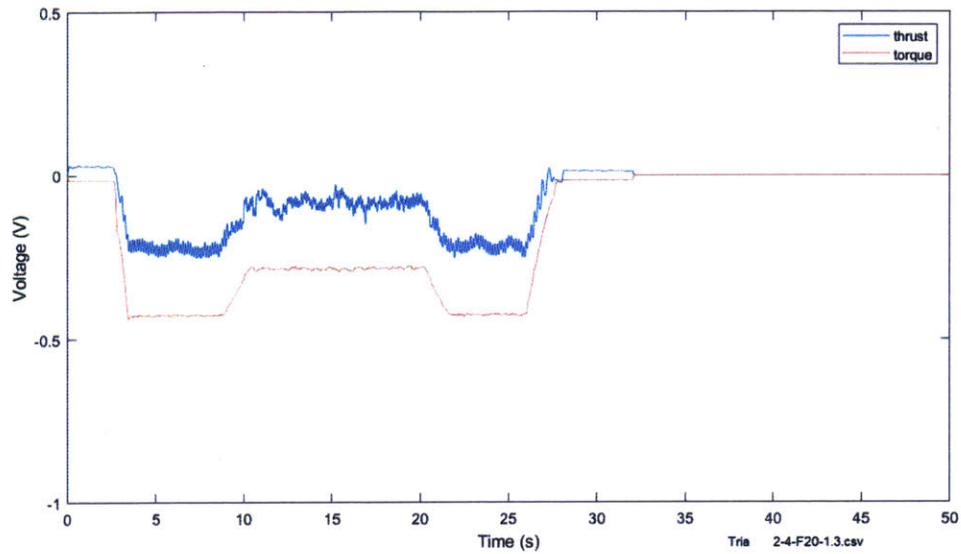
Figure 4-3: Filtered thrust and torque voltage at $V_A = 1.3m/s$ and motor driver frequency of 20 Hz.

constant speed but the test boat structure had to reach equilibrium. The response of the test boat structure can be seen from the thrust measurement. The thrust reaches a maximum just after the carriage accelerates to full speed where it then dips down below the run average before reaching a steady state. The period of this oscillation increased as carriage speed decreased.

K_Q Calculation: The average torque of the run was calculated from equation 2.2. The tare torque calculated from equation 4.1 was then subtracted from the run torque to get the resulting torque generated by the propeller. Values for $10K_Q$ were then calculated using equation 1.2.

K_T Calculation: Equation 2.1 was used to calculate thrust from voltage. The gain of the amplifier was set to 4000 and the excitation voltage was set to 10 V. This resulted in a very simple equation for thrust, $F_z = T = 63.63 * V_{fout}$. The data was then "zeroed" by adjusting the data by the difference in measured bollard thrust and expected bollard thrust (T_b). Finally, the drag of the propeller hub was subtracted from from the steady state thrust. Values for K_T were then calculated using equation

1.1.

K_T and K_Q Performance Curves: Values of K_T and $10K_Q$ were plotted against advance ratio J. A line was fit to each data set to create the performance curves. Typically, a curve would be faired to the data but in the case of the benchmark propeller the "curve" is mostly a straight line that curves down slightly at each end. The results from all 60 runs are plotted in Figure 4-4. Resulting values of $10K_Q$ had
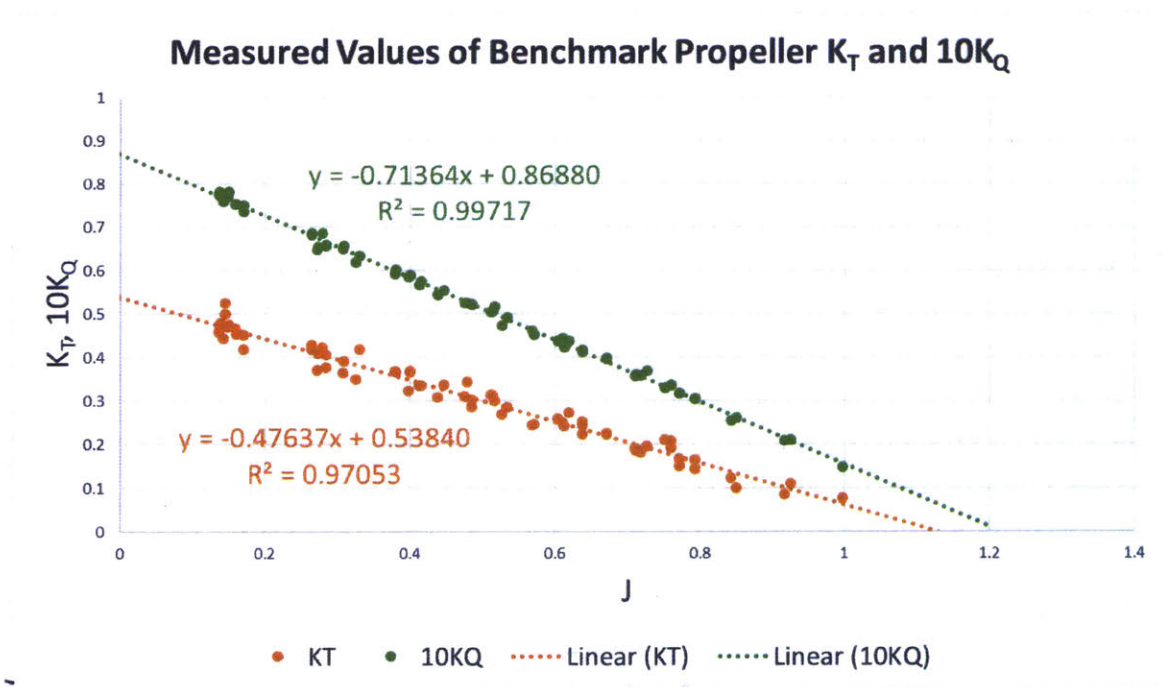
Figure 4-4: Measured values of benchmark K_T and $10K_Q$ plotted against J.

a strong linear trend with a small amount of variation. Values for K_T varied more than $10K_Q$ but followed the expected trend.

The performance curves fit to the measured values where then plotted and compared to the actually performance curves of the benchmark propeller as seen in Figure 4-5. A summary of these results can be found in Appendix G.
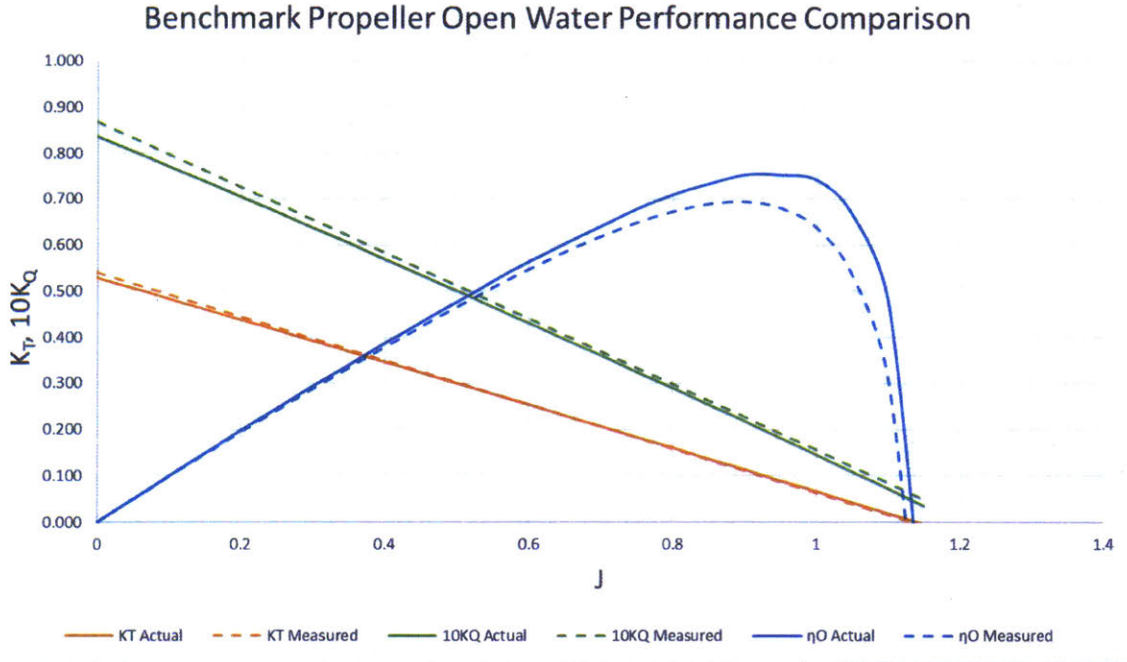
Figure 4-5: Benchmark open water performance curve comparison.

4.3 Benchmark Test Summary

The open water performance of the benchmark propeller was measured over a range of advance ratios from 0.15 to 1. The results of this test show close agreement with the actual performance of propeller model 4276. The percent difference between measured and expected values of thrust have a mean of 6.08% and a standard deviation of 5.37%. The percent difference between measured and expected values of torque have a mean of 2.97% and a standard deviation of 1.59%. To estimate the error in using a linear regression line as the performance curve, the standard error of the estimate (SEE) was calculated (Eq. 4.4). The SEE is the square root of the average squared deviation from the regression line. This error was 0.0198 for K_T and 0.0091 for $10K_Q$.

$$SEE = \sqrt{\frac{\sum_{i=1}^{N}(Y_i - (aX_i + b))^2}{N - 2}} \qquad (4.4)$$

Where Y_i and X_i are the coordinates of the data point, a is the slope of the regression line, b is the y-intercept of the regression line, and N is the number of data points.

4.4   Replica Propeller Testing and Results

The replica propeller was tested similar to the benchmark. Two runs were conducted at six different carriage speeds and 5 different motor driver frequencies plus three additional runs for a total of 63 runs. Motor driver frequencies were set to 18, 20, 22, 24, and 26 Hz and carriage speeds set to 0.25, 0.5, 0.75, 1, 1.3, and 1.6 m/s. Three additional runs were conducted at 28 Hz and carriage speeds of 1, 1.3, and 1.6 m/s. This testing approach again covered a range of advance ratios from approximately 0.15 to 1. The average Reynolds number of all 63 runs was 1.7×10^5.

4.4.1   Dummy Hub Measurements

Torque measurements using the dummy hub were taken at motor driver frequencies of 18, 20, 22, and 24 Hz. Measurements taken at 18 Hz were collected improperly and the results were not used. Result of the dummy hub measurements are plot in Figure 4-6.
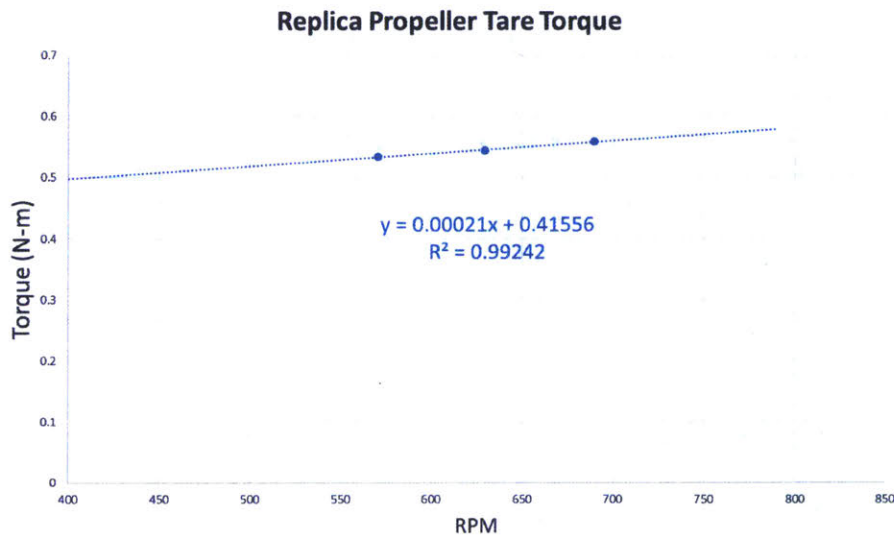
Figure 4-6: Replica dummy hub torque measurements.

Based on these measurements the following equation was used to zero the torque measurements.

$$Q_{tare} = 0.00021 * RPM + 0.4156 \qquad (4.5)$$

4.4.2 Bollard Measurements

Bollard measurements were taken at driver frequencies from 18 to 26 Hz in 2 Hz increments. The results of these measurments are plotted and compared to theoretical values and measured benchmark values in Figure 4-7.
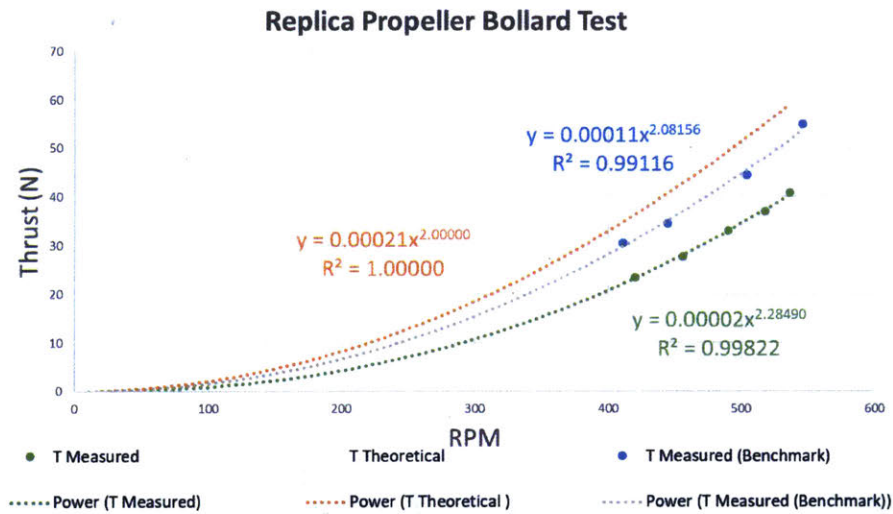
Figure 4-7: Replica bollard thrust measurements.

The following equations was used to calculated expected bollard thrust for each run.

$$T_{brep} = 0.000235 * RPM^{2.2849} \qquad (4.6)$$

4.4.3 Open Water Performance

After all 63 runs the data was analyzed in the same way and values for K_T and $10K_Q$ were calculated as previously discussed.

K_T and K_Q Performance Curves: Measured values of K_T and $10K_Q$ are plotted in Figure 4-8. The open water performance curves of the replica propeller compared

to the benchmark are presented in Figure 4-9. However, this comparison is not the most accurate. Therefore, a comparison of the expected as-built performance to the measured performance was made (Figure 4-10). The as-built geometry of the replica propeller must closely represents a Wageningen B3-68 with a P/D of 1.14. The tabulated results of this comparison can be found in Appendix G.

Measured Replica Propeller K_T and $10K_Q$

$$y = -0.68434x + 0.82565$$
$$R^2 = 0.99500$$

$$y = -0.42222x + 0.44252$$
$$R^2 = 0.96525$$
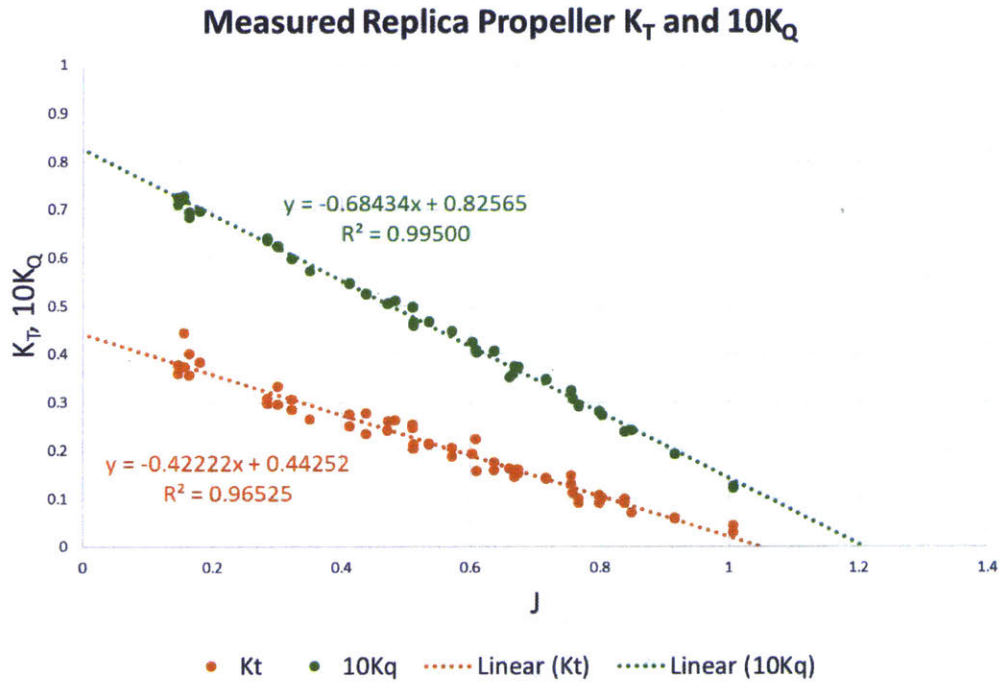
Figure 4-8: Measured values of replica K_T and $10K_Q$ plotted against J.

4.5 Replica Test Summary

The open water performance of the replica propeller was measured over a range of advance ratios from 0.15 to 1. The results of this test deviate significantly from the benchmark and CFD predictions. The percent difference between measured and benchmark values of thrust have a mean of 32.1% and a standard deviation of 14.25%. The percent difference between measured and benchmark values of torque have a mean of 3.6% and a standard deviation of 3.1%. The SEE was 0.0191 for K_T and 0.0116 for $10K_Q$.

58
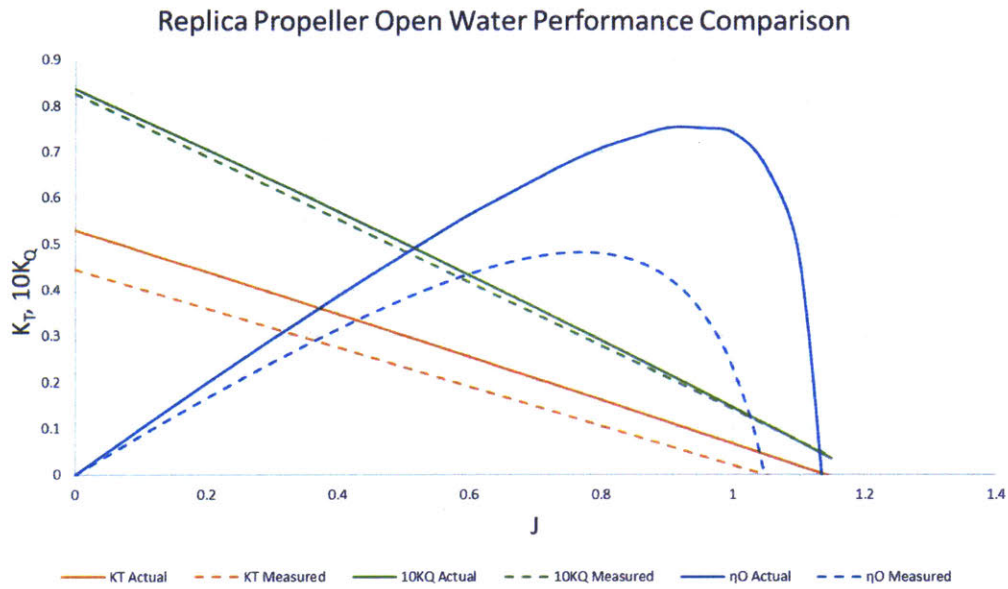
Figure 4-9: Replica open water performance curve comparison, benchmark vs. measured.
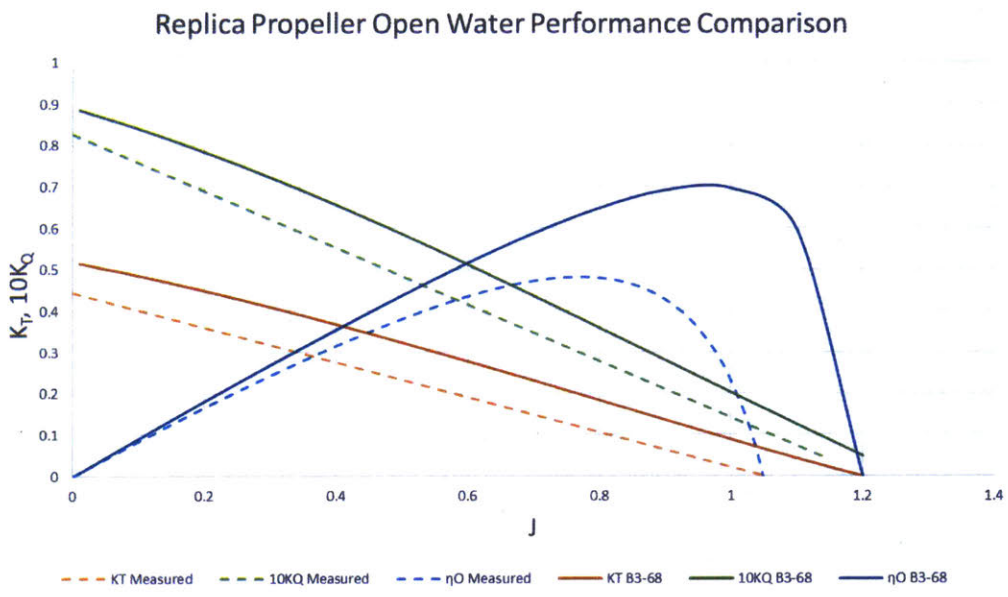
Figure 4-10: Replica open water performance curve comparison, B3-68 vs. measured.

THIS PAGE INTENTIONALLY LEFT BLANK

Chapter 5

Discussion

5.1 Open Water Test Boat Performance

The test boat performed reasonable well but fell short of two important requirements. The first is to test at a Reynolds number of 2×10^5 and the second is to maintain a constant RPM throughout the test. While in certain cases a Reynolds number of greater than 2×10^5 (overcritical) was achieved, on average this threshold was not met for various reasons. The Reynolds number of a given test is a function of the rate at which the propeller rotates and the speed it is towed which is dependent on the torque generated by the propeller and the power of the drive motor. The power of the drive motor was the most limiting factor. The majority of runs were conducted at or near the motors torque limit of 2 n-m. It is possible that a different propeller could be tested at an overcritical level, specifically one with a greater chord length and lower P/D. However, this possibility is marginal and would include a small number of propellers.

It was initially expected that the PWM signal supplied by the motor driver would maintain a constant motor RPM through the run. In practice the motor RPM was not completely constant even after the carriage reached a steady speed. Small fluctuations in RPM were observed throughout each run. These small fluctuations are likely due to variations in load and the fact that the motor was operating at or near its torque limit. While these fluctuations are small their effects can be significant.

5.2 Measurement Uncertainty

A number of factors in a propeller open water test contribute to the uncertainty of the experimental measurements. This uncertainty is a result of the error associated with the measurement of propeller geometry, carriage speed, rate of revolution, thrust/torque, and water temperature (density). In general, the design and construction of the test boat described in this thesis created a significant amount of uncertainty in the measurement of RPM and thrust. The error associated with measuring water temperature was assumed to be negligible.

The method of using a Hall effect sensor to measuring RPM proved to be a sound method. However, the control of propeller RPM was not adequate. Small fluctuation in RPM were observed over the course of a run. These small fluctuations in RPM effect the range over which measurements of thrust and torque could be taken.

The placement and in situ calibration of the thrust sensor cause the greatest amount of uncertainty. The thrust sensor is positioned a good distance from the propeller requiring the support of three bearings, two of which are roller bearings and the other a sleeve bearing. The roller bearings are designed to provide support in the radial direction. Due to the play or "slop" of these bearings the axial resistance of the roller bearings is negligible. This is because the axial deflection of the thrust sensor is much less than the play in the roller bearings. The stiffness in the Fz direction of the MC1 sensor is $1 \times 10^7 N/m$ resulting in a max deflection of $3\mu m$ at 30 N of force (resultant max thrust). The sleeve bearing on the other hand exerts an appreciable amount of axial resistance, or binding. To provide lubrication a thin layer of oil is produce from the friction between the spinning shaft and the oil-embedded bronze sleeve. Because of this the resistance of the sleeve bearing is a function of RPM, fit tolerance, and shaft alignment. The axial force exerted by the rotation of the shaft was measured to be approximately 12.75 N. This measurement was taken while slowly rotating the shaft 360 degrees by hand. The axial force appeared to decrease as shaft rotation increased. In the absence of a method to conduct a dynamic calibration while submerged, it is difficult to estimate the effects these factors have on the in situ

calibration of the thrust sensor and the resulting error in thrust measurements.

The torque sensor provided the most certainty and was often used in preliminary tests as a check for the thrust measurement. Uncertainty was reduce through the use of the NIST certified calibration provided by the manufacture. The calibration data showed minuscule amounts of non-linear error. Uncertainty was further reduce through the observed accuracy in repeated experiments.

5.3   Benchmark Propeller

The must likely explanation of the discrepancy between measured and actual torque of the benchmark propeller is due to testing at undercritical Reynolds numbers. For the benchmark test Reynolds numbers of 2×10^5 were reached at advance ratios of 0.6 and greater. As a result the measurement accuracy increase above this threshold. It is well know from aerofoil testing that at undercritical Reynolds numbers flow separation is delayed causing high pressure resistance and a decrease in lift. This translates to an increase in torque and a decrease in thrust for a undercritical propeller. While this explains the trend in torque it does not explain the trend in thrust. The inaccuracy of the thrust measurement can be explained by the various uncertainties discussed previously. The thrust is suspected to be slightly lower at lower advance ratios than what was measures. This is a result of not being able to conduct an accurate dynamic calibration. For both thrust and torque, taking measurements over a greater range of advance ratios would provide greater fidelity.

5.4   Replica Propeller

The factors effecting measurement accuracy remain the same for the replica propeller but are compounded by errors in the replica propellers geometry. The largest factor was the orientation of the propeller blades. The blades pitch was increased in a crude sense by rotating the blade and hub about the propeller reference line (approximately) resulting in a suboptimal orientation. The propeller blades are no longer

oriented to the flow as designed resulting in decreased lift and increased drag. The blades shape also has a strong effect on the flow characteristics around the propeller blade. The relatively small errors in blade thickness, discussed in Ch. 3, changes the chord to thickness distribution which effects the pressure distribution of the blade. A change in pressure distribution changes the transition point from laminar to turbulent flow thus changing the thrust and torque generated by the propeller.

With so many factors effecting thrust and torque it is difficult to estimate the extent to which each factor has effected the measurements without systematically varying each one. An exact as-built model of the replica propeller was not created and thus the geometrical inaccuracies developed through the manufacturing processes can not be assessed in exact detail.

Chapter 6

Conclusion

The purpose of this project was to build a propeller open water test boat to be used in MIT's towing tank. A subsequent goal was to evaluate the feasibility of using a 3D printed model propeller for testing. This report describes the design of a propeller open water test boat. The test boats performance was validated using a benchmark propeller of known open water performance characteristics. The test boat performed well and was able to measure the open water performance of the benchmark propeller within a small percentage of error. However, a few modifications to the design most be made to eliminate measurement uncertainty and to achieve the recommended performance set by the ITTC.

This report also discusses the manufacturing of a model propeller using an benchtop SLA 3D printer. The open water performance of the 3D printed propeller was measured and found to deviate significantly from the expected performance. The poor performance of the printed propeller can be attributed mostly to geometrical inaccuracies of the propeller. These inaccuracies were a result of assembling the propeller one blade at a time. Ultimately, the process of manufacturing an in-house model propeller using a benchtop 3D printer was determined to be feasible. However, care should be taken to ensure proper blade symmetry and orientations are maintain if each blade is printed separately. The greatest amount of difficulty was found in manufacturing a propeller to the geometrical precision required to conduct a valid open water test.

6.1 Recommendations for Future Work

The leading recommendation is to make a few modifications to the test boat design in order to eliminated sources of measurement uncertainty. The AMTI MC1 sensor used to measure thrust is an excellent sensor but because it was incorporated late in the design its full capacity is not being utilized. The first modification is to reposition the thrust sensor to a position closer to the propeller and in-line with the propeller shaft. This could be done by splitting the propeller shaft in two section and coupling the two section together with the sensor via a flanged connection. The sensor wire would then be routed through the hollow aft shaft section to a slip ring. This setup would allow for the direct measurement of thrust and could also be used to measure torque. Another recommended modification is to upgrade the drive motor to one with more power. The driver for this motor should also be capable of maintaining a constant RPM throughout the run.

Another recommendation is to develop a method of conducting a dynamic in situ calibrations of the thrust sensor. This calibration should be conducted by apply loads in the positive and negative x direction while the shaft is spinning.

As many experimental research projects go, more testing can always be done. Further testing of a 3D printed propeller is necessary to fully understand the value a 3D printed propeller could add to future research. An avenue for future work could be to develop a better process to manufacture a 3D printed model propeller.
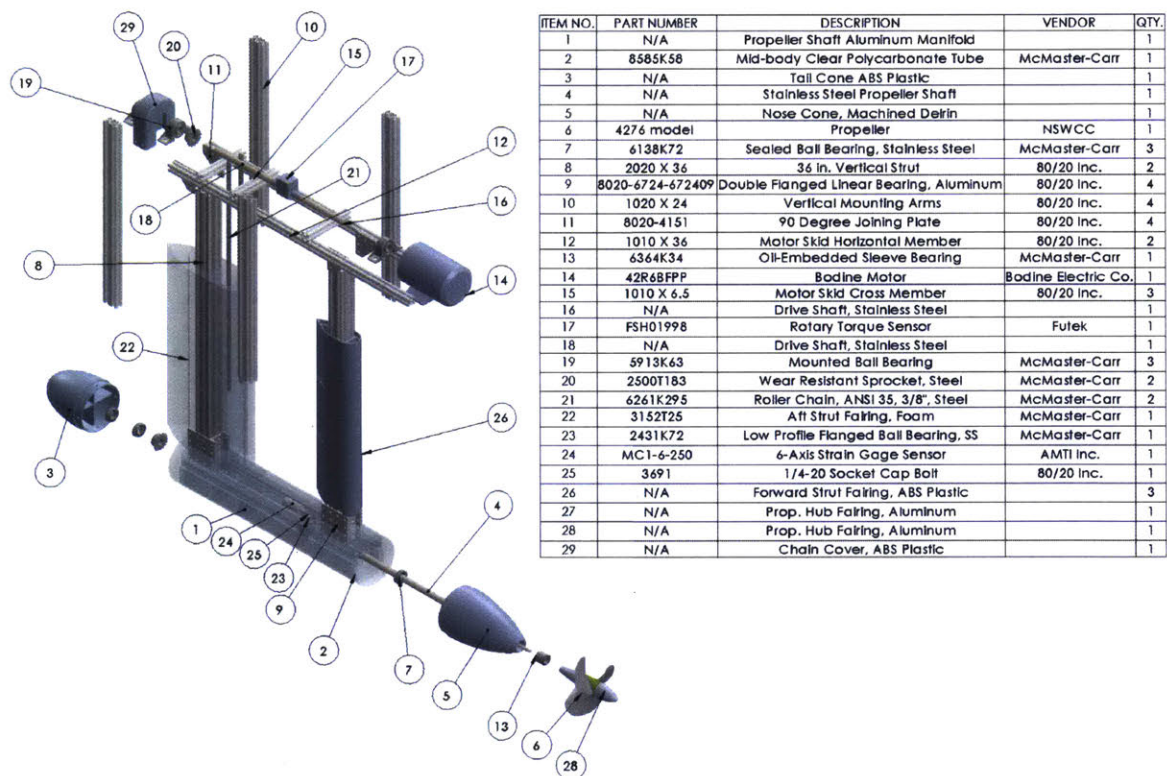
Appendix A

Final Propeller Boat Assembly

ITEM NO.	PART NUMBER	DESCRIPTION	VENDOR	QTY.
1	N/A	Propeller Shaft Aluminum Manifold		1
2	8585K58	Mid-body Clear Polycarbonate Tube	McMaster-Carr	1
3	N/A	Tail Cone ABS Plastic		1
4	N/A	Stainless Steel Propeller Shaft		1
5	N/A	Nose Cone, Machined Delrin		1
6	4276 model	Propeller	NSWCC	1
7	6138K72	Sealed Ball Bearing, Stainless Steel	McMaster-Carr	3
8	2020 X 36	36 in. Vertical Strut	80/20 Inc.	2
9	8020-6724-672409	Double Flanged Linear Bearing, Aluminum	80/20 Inc.	4
10	1020 X 24	Vertical Mounting Arms	80/20 Inc.	4
11	8020-4151	90 Degree Joining Plate	80/20 Inc.	4
12	1010 X 36	Motor Skid Horizontal Member	80/20 Inc.	2
13	6364K34	Oil-Embedded Sleeve Bearing	McMaster-Carr	1
14	42R6BFPP	Bodine Motor	Bodine Electric Co.	1
15	1010 X 6.5	Motor Skid Cross Member	80/20 Inc.	3
16	N/A	Drive Shaft, Stainless Steel		1
17	FSH01998	Rotary Torque Sensor	Futek	1
18	N/A	Drive Shaft, Stainless Steel		1
19	5913K63	Mounted Ball Bearing	McMaster-Carr	3
20	2500T183	Wear Resistant Sprocket, Steel	McMaster-Carr	2
21	6261K295	Roller Chain, ANSI 35, 3/8", Steel	McMaster-Carr	2
22	3152T25	Aft Strut Fairing, Foam	McMaster-Carr	1
23	2431K72	Low Profile Flanged Ball Bearing, SS	McMaster-Carr	1
24	MC1-6-250	6-Axis Strain Gage Sensor	AMTI Inc.	1
25	3691	1/4-20 Socket Cap Bolt	80/20 Inc.	1
26	N/A	Forward Strut Fairing, ABS Plastic		3
27	N/A	Prop. Hub Fairing, Aluminum		1
28	N/A	Prop. Hub Fairing, Aluminum		1
29	N/A	Chain Cover, ABS Plastic		1

Figure A-1: Final Propeller Boat Assembly and Bill of Materials

THIS PAGE INTENTIONALLY LEFT BLANK

Appendix B

MC1-6-250 Specification

MC1   FORCE/TORQUE SENSOR

APPLICATIONS
The MC1 force/torque sensor is AMTI's smallest multi-component sensor and is particularly suitable for underwater applications requiring simultaneous measurement of several forces and moments. Common applications for this transducer include research and development with underwater models, tow tanks, robotics, testing machines, and biomechanics.

DESCRIPTION
AMTI's MC1 force/torque sensor is specifically designed for the precise measurement of under water forces and moments. The sensor measures the three orthogonal force components along the X, Y, and Z axes, and the moments about these axes, producing a total of six outputs. The characteristics of this sensor make it ideal for research and testing environments; it has high stiffness, high sensitivity, low cross-talk, excellent repeatability and long term stability. It is simple, easy to use, and is available in a 500 pound (2200 Newton) vertical capacity.

The body of the load cell is manufactured from heat treated 17-4 PH stainless steel, and has mounting surfaces equipped with threaded holes.

CALIBRATION
Each sensor is inspected and tested at AMTI's calibration facility. The calibration procedure provides a detailed sensitivity matrix and a complete test of all system components, including the amplifier and the connecting cable if ordered together.

AMPLIFICATION
The MC1 Force/Torque Sensor incorporates strain gages mounted on a precision strain element to measure forces and moments. As with most conventional strain gage transducers, bridge excitation and signal amplification are required. AMTI's SGA or MCA amplifiers are high gain devices which provide excitation and amplification for multiple channels in one convenient package. The rack mountable MCA-6, or the desktop SGA6-4 provide the six channels of amplification required by the sensor. These amplifiers process the sensor's low-level signals and provide outputs suitable for an A/D converter so that the data can be stored and processed by a computer.

CUSTOM
AMTI also offers other transducers to meet your specific needs. Units with larger surface areas are available, and sensors with capacities as high as 3,000,000 pounds (13,345,000 Newtons) have also been constructed. Units are available in waterproof versions and in various sizes, load capacities, sensitivities, and materials.
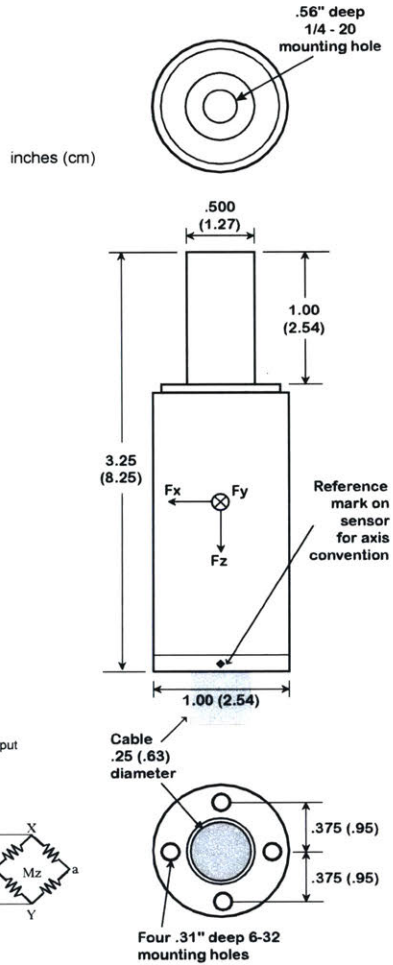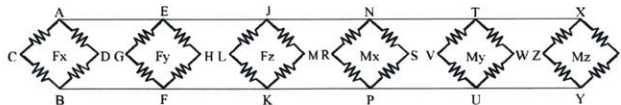
ISO 9001 CERTIFIED

MC1 FORCE/TORQUE SENSOR

MC1 SPECIFICATIONS	500
Fx, Fy Capacity, lb, (N)	250 (1100)
Fz Capacity, lb, (N)	500 (2200)
Mx, My Capacity, in*lb, (Nm)	100 (11)
Mz Capacity, in*lb, (Nm)	100 (11)
Fz Sensitivity, µV/[V*lb], (µV/[V*N])	0.9 (0.20)
Fx, Fy Sensitivity, µV/[V*lb], (µV/[V*N])	3.5 (0.78)
Mx, My Sensitivity, µV/[V*in*lb], (µV/[V*Nm])	7.0 (62.0)
Mz Sensitivity, µV/[V*in*lb], (µV/[V*Nm])	7.0 (62.0)
Fz Stiffness, $X10^5$ lb/in, ($X10^7$ N/m)	9.0 (15.75)
Fx, Fy Stiffness, $X10^5$ lb/in, ($X10^7$ N/m)	0.5 (0.86)
Mz Stiffness, $X10^4$ in*lb/radian, ($X10^4$ Nm/radian)	2.0 (0.23)

inches (cm)

.56" deep
1/4 - 20
mounting hole

.500 (1.27)

1.00 (2.54)

3.25 (8.25)

Fx Fy
Fz

Reference mark on sensor for axis convention

1.00 (2.54)

Cable .25 (.63) diameter

.375 (.95)

.375 (.95)

Four .31" deep 6-32 mounting holes

WIRING FOR MC1

+ Excitation

- Output   + Output

- Excitation

If wired to a connector:

A   E   J   N   T   X
C Fx D G Fy H L Fz M R Mx S V My W Z Mz a
B   F   K   P   U   Y
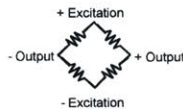
All excitations are wired in parallel.

GENERAL SPECIFICATIONS
Weight: 0.20 lb (89 g)
Recommended Excitation: 10V or less
Crosstalk: Less than 2% on all channels
Temperature Range: 0 to 125°F, (-17 to 52°C)
Fx, Fy, Fz hysteresis: ± 0.2 % Full Scale Output
Fx, Fy, Fz non-linearity: ± 0.2% Full Scale Output

ISO 9001 CERTIFIED

AMTI

ADVANCED MECHANICAL TECHNOLOGY, INC.
176 WALTHAM STREET WATERTOWN, MA 02472-4800
TEL: (617) 926-6700 ● (800) 422-AMTI ● FAX: (617) 926-5045
email: sales@amtimail.com ● web: www.amtiweb.com

THIS PAGE INTENTIONALLY LEFT BLANK

Appendix C

Sensor Calibration Data

Table B.1   Main Sensitivities and Coordinates

SN   M4657   **11/16/2006 15:12**

English Units

Main Sensitivity

Fx	6.9789	microVolt/Voltexc-lb
Fy	6.9722	microVolt/Voltexc-lb
Fz	1.7477	microVolt/Voltexc-lb
Mx	13.7426	microVolt/Voltexc-in-lb
My	13.6297	microVolt/Voltexc-in-lb
Mz	13.4990	microVolt/Voltexc-in-lb

Metric Units

Main Sensitivity

Fx	1.5690	microVolt/Voltexc-N
Fy	1.5675	microVolt/Voltexc-N
Fz	0.3929	microVolt/Voltexc-N
Mx	121.6358	microVolt/Voltexc-N-m
My	120.6366	microVolt/Voltexc-N-m
Mz	119.4800	microVolt/Voltexc-N-m

Transducer Axis Origin

Coordinate

English

Xo=	-1.98E-02	inches
Yo=	-5.29E-02	inches
Zo=	1.43E+00	inches

Metric

Xo=	-0.50292	mm
Yo=	-1.34366	mm
Zo=	36.2585	mm

Table C.1: AMTI Provided Sensitivities and Coordinates for MC1-6-250-M4657

Table C.2: Futek TRS600 Calibration Data

| Clockwise		Counterclockwise	
N-m	Volts	N-m	Volts
0	0.000	0	0.000
3.389	-0.844	3.389	0.846
6.779	-1.689	6.779	1.694
10.168	-2.534	10.168	2.539
13.558	-3.378	13.558	3.384
16.947	-4.223	16.947	4.23
19.997	-4.985	19.997	4.993

Appendix D

FUTEK TRS600 Specification

FUTEK
ADVANCED SENSOR TECHNOLOGY, INC

Rotary Torque Sensor – Non-Contact Shaft-to-Shaft

FEATURES

- Utilizes strain gauge technology
- Compact size
- Can operate up to 12000 RPM (9-89 in-lb)

Active end

– Output (CCW)
+ Output (CW)
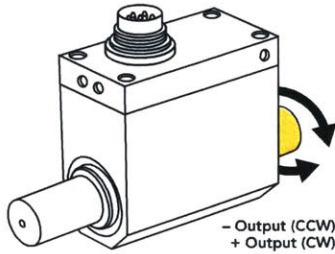
SPECIFICATIONS

PERFORMANCE

Nonlinearity	±0.2% of RO
Hysteresis	±0.1% of RO
Nonrepeatability	±0.2% of RO
Rotational Speed	12000 Max (9-89 in-lb) 9000 Max (177-885 in-lb)

ELECTRICAL

Rated Output (RO)	±5 VDC
Excitation (VDC or VAC)	11–26 VDC, 1 Watt
Connection	12 pin Binder Series #581 (09-0331-90-12)

MECHANICAL

Weight (approximate)	0.6 lb [0.28 kg] (9-89 in-lb) 1.1 lb [0.50 kg] (177-443 in-lb) 2.3 lb [1.06 kg] (885 in-lb)
Safe Overload	150% of RO
Material	Aluminum (Housing) Alloy Steel (Shaft)
IP Rating	IP40

TEMPERATURE

Operating Temperature	−13 to 176°F (−25 to 80°C)
Compensated Temperature	41 to 122°F (5 to 50°C)
Temperature Shift Zero	±0.01% of RO/°F (±0.02% of RO/°C)
Temperature Shift Span	±0.01% of RO/°F (±0.02% of RO/°C)

CALIBRATION

Calibration Test Excitation	12 VDC
Calibration (standard)	Certificate of Conformance
Calibration (available)	5-pt CW & CCW
Shunt Calibration Value	With sensor fully connected apply 11–26 VDC to Pins A & K to generate 5 VDC nom output

CONFORMITY

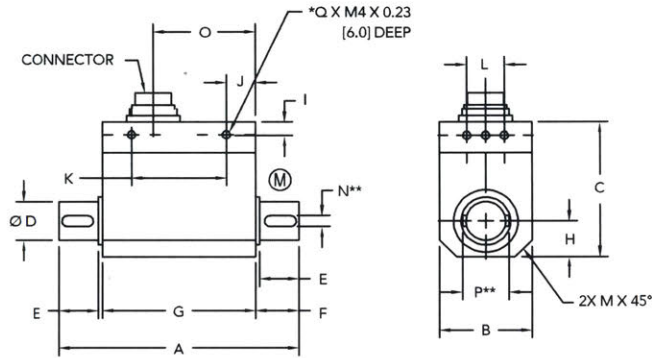|	
RoHS	2014/30/EU
CE	Declaration of Conformity

CONNECTOR CODES

| PIN	COLOR	DESCRIPTION
A	Yellow	Shunt Cal (gnd)
C	Green	Signal
D	White	Return (Signal)
E	Black	Ground
F	Red	Power
K	Purple	Shunt Cal
M	Floating	Shield

DIMENSIONS inches [mm]

*Q X M4 X 0.23 [6.0] DEEP
CONNECTOR

Ⓜ = MEASURING SIDE

* ANTI-ROTATION HOLES. NOT TO BE USED TO SUPPORT LOAD.
** FEATHER KEYWAYS PER DIN 6885, KEYWAYS COME PRE-INSTALLED

MASS MOMENT OF INERTIA (kg x cm²)

ITEM #	Measuring End	Drive End
FSH01994	0.0146	0.0147
FSH01995	0.0146	0.0147
FSH01996	0.015	0.015
FSH01997	0.015	0.015
FSH01998	0.061	0.073
FSH01999	0.062	0.075
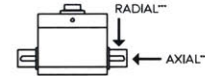
CAPACITIES

ITEM #	Nm [in-lb]	A	B	C	ØD	E	F	G	H	I	J	K	L	M	N**	O	P**	Q*	*** Max Axial Force lb [N]	*** Max Radial Force lb [N]	Torsional Stiffness Nm/rad
FSH01994	1 [9]																		4.5 [20]	1 [5]	317
FSH01995	2 [18]	3.62 [92]	1.10 [28]	2.04 [52]	0.394 [10] g6	0.63 [16]	0.67 [17]	2.28 [58]	0.55 [14]	0.19 [5]	0.43 [11]	-	0.31 [8]	0.32 [8]	-	1.46 [37]	-	6	11 [50]	1 [5]	317
FSH01996	5 [44]																			2 [10]	855
FSH01997	10 [89]																		34 [150]	4.5 [20]	855
FSH01998	20 [177]	4.25 [108]	1.49 [38]	2.28 [58]	0.748 [19] g6	1.18 [30]	1.26 [32]	1.73 [44]	0.75 [19]	0.24 [6]	0.86 [22]	-	0.40 [10]	0.236 [6]	0.87 [22]	0.945 [24]	3			7 [30]	5450
FSH01999	50 [443]																		45 [200]	11 [50]	9500
FSH02730	100 [885]	4.92 [125]	2.28 [58]	2.99 [76]	1.102 [28] g6	1.06 [27]	1.20 [30.5]	2.52 [64]	1.14 [29]	0.19 [5]	0.55 [14]	1.97 [50]	1.18 [30]	-	0.315 [8] p9	1.57 [40]	1.34 [34]	8	90 [400]	56 [250]	

CE RoHS ANSI Z540-1 ISO 17025 ISO 9001 ISO 13485 U.S. Manufacturer

THIS PAGE INTENTIONALLY LEFT BLANK

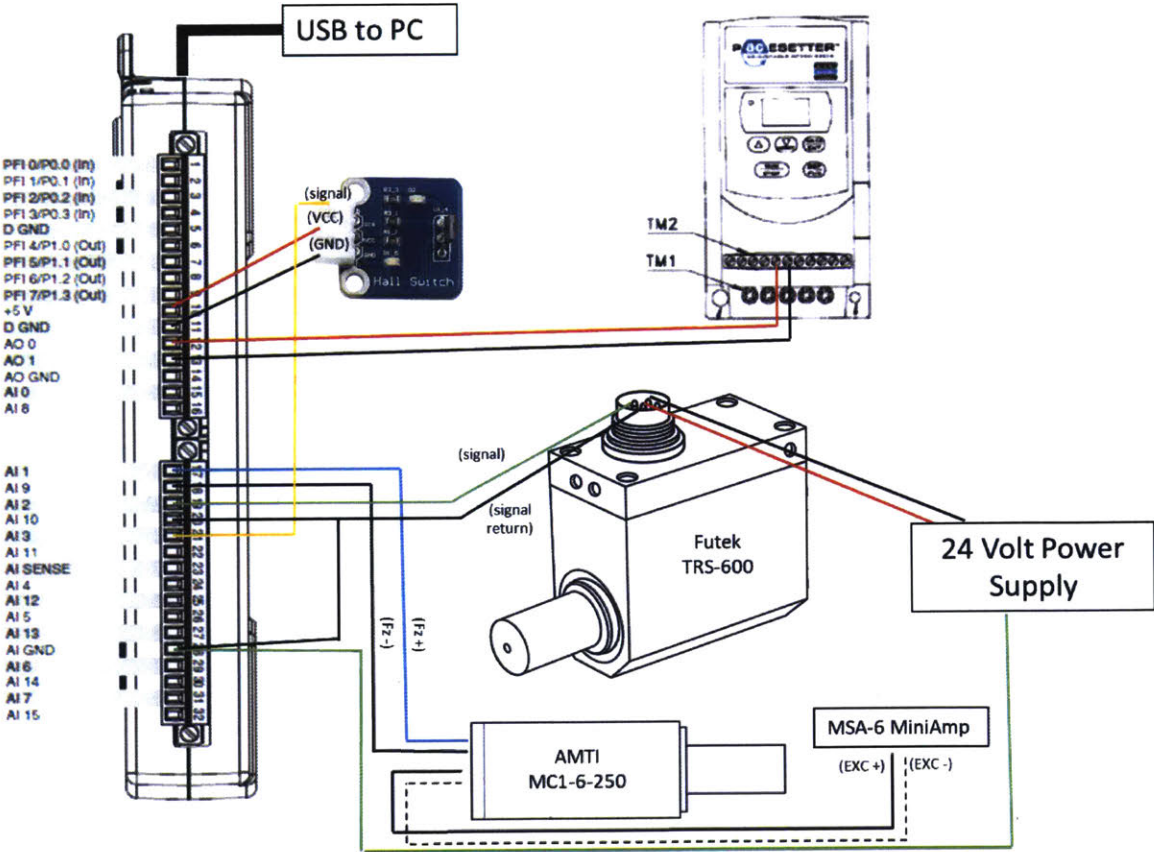# Appendix E

Propeller Boat Wiring Schematic

Figure E-1: Propeller boat wiring schematic

THIS PAGE INTENTIONALLY LEFT BLANK

Appendix F

Model 4276 Open Water Data

Open Water Coefficients Props 4276 & 4277 16 Feb. 1967, Dia. 7.623, P/D 1.070, Blades 3			
J	Kt	10Kq	ETA O
0	0.528	0.836	0.000
0.05	0.506	0.803	0.050
0.1	0.483	0.77	0.100
0.15	0.46	0.737	0.149
0.2	0.438	0.704	0.198
0.25	0.415	0.67	0.246
0.3	0.392	0.636	0.294
0.35	0.369	0.603	0.341
0.4	0.346	0.568	0.388
0.45	0.323	0.534	0.433
0.5	0.3	0.5	0.477
0.55	0.277	0.465	0.521
0.6	0.254	0.43	0.564
0.65	0.23	0.395	0.602
0.7	0.207	0.36	0.641
0.75	0.184	0.324	0.678
0.8	0.161	0.289	0.709
0.85	0.137	0.253	0.733
0.9	0.114	0.217	0.753
0.95	0.09	0.181	0.752
1	0.067	0.144	0.741
1.05	0.043	0.108	0.665
1.1	0.019	0.071	0.468
1.15	-0.004	0.034	-0.215

THIS PAGE INTENTIONALLY LEFT BLANK

Appendix G

Open Water Performance

J	Benchmark Propeller Open Water Performance Comparison					
	Actual K_T	Measured K_T	Actual $10K_Q$	Measured $10K_Q$	Actual η_O	Measured η_O
0	0.528	0.538	0.836	0.869	0.000	0.000
0.05	0.506	0.515	0.803	0.833	0.050	0.049
0.1	0.483	0.491	0.770	0.797	0.100	0.098
0.15	0.460	0.467	0.737	0.762	0.149	0.146
0.2	0.438	0.443	0.704	0.726	0.198	0.194
0.25	0.415	0.419	0.670	0.690	0.246	0.242
0.3	0.392	0.395	0.636	0.655	0.294	0.288
0.35	0.369	0.372	0.603	0.619	0.341	0.334
0.4	0.346	0.348	0.568	0.583	0.388	0.380
0.45	0.323	0.324	0.534	0.548	0.433	0.424
0.5	0.300	0.300	0.500	0.512	0.477	0.467
0.55	0.277	0.276	0.465	0.476	0.521	0.508
0.6	0.254	0.253	0.430	0.441	0.564	0.547
0.65	0.230	0.229	0.395	0.405	0.602	0.584
0.7	0.207	0.205	0.360	0.369	0.641	0.618
0.75	0.184	0.181	0.324	0.334	0.678	0.648
0.8	0.161	0.157	0.289	0.298	0.709	0.672
0.85	0.137	0.133	0.253	0.262	0.733	0.689
0.9	0.114	0.110	0.217	0.227	0.753	0.693
0.95	0.090	0.086	0.181	0.191	0.752	0.680
1	0.067	0.062	0.144	0.155	0.741	0.636
1.05	0.043	0.038	0.108	0.120	0.665	0.534
1.1	0.019	0.014	0.071	0.084	0.468	0.301
1.15	-0.004	-0.009	0.034	0.048	-0.215	-0.358

	Replica Propeller Open Water Performance Comparison					
	Replica	B3-68	Replica	B3-68	Replica	B3-68
J	K_T	K_T	$10K_Q$	$10K_Q$	η_O	η_O
0	0.44252	0.514158	0.82565	0.886328	0	0.009233
0.05	0.421409		0.791433		0.042372	
0.1	0.400298	0.484587	0.757216	0.840939	0.084136	0.091712
0.15	0.379187		0.722999		0.125207	
0.2	0.358076	0.448345	0.688782	0.784662	0.165479	0.181878
0.25	0.336965		0.654565		0.204829	
0.3	0.315854	0.409019	0.620348	0.722968	0.243104	0.270126
0.35	0.294743		0.586131		0.280115	
0.4	0.273632	0.367104	0.551914	0.656616	0.315628	0.355924
0.45	0.252521		0.517697		0.349345	
0.5	0.23141	0.323093	0.48348	0.586365	0.380885	0.43848
0.55	0.210299		0.449263		0.40975	
0.6	0.189188	0.277482	0.415046	0.512976	0.43528	0.516545
0.65	0.168077		0.380829		0.456575	
0.7	0.146966	0.230764	0.346612	0.437208	0.47238	0.588028
0.75	0.125855		0.312395		0.480892	
0.8	0.104744	0.183435	0.278178	0.35982	0.47942	0.649091
0.85	0.083633		0.243961		0.463763	
0.9	0.062522	0.135988	0.209744	0.281573	0.426978	0.691788
0.95	0.041411		0.175527		0.35671	
1	0.0203	0.088919	0.14131	0.203225	0.228635	0.696364
1.05	-0.00081		0.107093		-0.01266	
1.1	-0.02192	0.042721	0.072876	0.125537	-0.52663	0.59578
1.15	-0.04303		0.038659		-2.03737	

Bibliography

[1] "Model Manufacture, Propeller Models Terminology and Nomenclature for Propeller Geometry," in *22nd ITTC - Recommended Procedures and Guidelines*, pp. 1–21, 2008.

[2] "Open Water Test," in *28th ITTC - Recommended Procedures and Guidelines*, 2014.

[3] "Testing and Extrapolation Methods Propulsion, Propulsor Open Water Test," in *23rd ITTC - Recommended Procedures*, pp. 1–9, 2002.

[4] M. Oosterveld and P. V. Oosanen, "Further Computer-Analyzed Data of the Wageningen B-Screw Series," in *IV International Symposium on Ship Automation*, 1974.

[5] M. Bernitsas, D. Ray, and P. Kinley, "Kt, Kq and Efficiency curves for the Wageningen B-series Propellers," tech. rep., University of Michigan, 1981.

[6] D. Capozzo and A. Peak, "Design of a Propeller Boat for Open-water Testing in the Robinson Model Basin at Webb Institute," 2000.

[7] N. Dombrowski, D. Frauenberger, and K. Van Veen, "Design and Construction of a New Open-water Testing System for the Robinson Model Basin," 2002.

[8] J. Lorio, "Open Water Testing of a Surface Piercing Propeller with Varying Submergence, Yaw Angle and inclination Angle," Master's thesis, Florida Atlantic University, 2010.

[9] "Propeller Model Accuracy," in *28th ITTC - Recommended Procedures and Guidelines*, 2017.

[10] I. Dagres, "Simulation-Guided Lattice Geometry Optimization of Metal Marine Propeller for Additive Manufacturing," Master's thesis, Massachusetts Institute of Technology, 2019.

[11] K. Lim, "Hydrodynamic Performance and Vortex Shedding of a Biologically Inspired Three-Dimensional Flapping Foil," Master's thesis, Massachusetts Institute of Technology, 2005.